

the two antagonal Néel states. Starting from one of them and reaching its antipole implies far more than a small deviation. Hence, a suitable bosonic representation is required for which we use Schwinger bosons [18, 22–25].

This representation does not use long-range order in a Néel state as reference state so that it can describe even the disordered state. Thus, even on the mean-field level, Schwinger bosons can capture large deviations from one of the ground states. We are aware that Schwinger boson mean-field theory may display pathologies in form of spurious first-order transitions. But these are not likely in unfrustrated low-dimensional systems [26]. We use Schwinger bosons to describe the isotropic and anisotropic systems at equilibrium initially. Then, we demonstrate how this representation can be used to simulate the switching of the sublattice magnetization by means of an external magnetic field. We analyze how the system changes after the rotation and how the anisotropy influences the switching. Thereby our study provides a basis for further theoretical investigations regarding the full control of quantum antiferromagnets which in turn is expected to guide further experimental investigations.

The article is set up as follows. After this Introduction, Sect. II introduces the model and its bosonic representation by Schwinger bosons. Then, Sect. III briefly recalls the corresponding mean-field theory in equilibrium for the isotropic and the anisotropic Heisenberg antiferromagnet. Subsequently, we derive the equations of motion describing the dynamics in applied magnetic fields which induce precessional motion in Sect. IV. Finally, we summarize our results in the Conclusions V.

II. HEISENBERG MODEL AND ITS SCHWINGER BOSON REPRESENTATION

A. Heisenberg model and its Hamiltonoperator

We consider here the (an)isotropic Heisenberg model on a square lattice for a quantum antiferromagnet with localized spins $S = 1/2$. Its Hamilton operator reads

$$\mathcal{H} = \sum_{\langle i,j \rangle} \{ J_{xy} (S_i^x S_j^x + S_i^y S_j^y) + J_z S_i^z S_j^z \}, \quad (1)$$

where i and j label sites of the underlying lattice, the sum runs over pairs of nearest neighbors counting each pair only once. The operators S_i^α are the usual operators of the spin component α at site i ; the couplings J_z and J_{xy} are both antiferromagnetic, i.e., positive. We focus on the easy-axis model taking $J_z = J$ as energy unit and defining the ratio $\chi = J_{xy}/J_z \in [0, 1]$ so that the Hamiltonian can be rewritten to

$$\mathcal{H} = J \sum_{\langle i,j \rangle} \{ \chi (S_i^x S_j^x + S_i^y S_j^y) + S_i^z S_j^z \} \quad (2a)$$

$$= J \sum_{\langle i,j \rangle} \left\{ \frac{\chi}{2} (S_i^+ S_j^- + S_i^- S_j^+) + S_i^z S_j^z \right\}, \quad (2b)$$

where the spin ladder operators are used in the last step.

For finite anisotropy $\chi < 1$, the magnons display a finite energy gap $\Delta(\chi) > 0$. In turn, the spin-spin correlation length ξ becomes finite following the estimate

$$\xi(\chi) = \frac{v}{\Delta(\chi)}, \quad (3)$$

where v is the spin-wave velocity. Below, we will perform a calculation for finite clusters with linear dimension L . These will reflect the thermodynamic, infinite size results whenever $L \gg \xi$ holds.

A uniform magnetic field can be included by adding the term

$$\mathcal{H}_{\text{uni}} = -\mathbf{h} \cdot \sum_i \mathbf{S}_i, \quad (4)$$

while an alternating (staggered) magnetic field is accounted for by adding

$$\mathcal{H}_{\text{alt}} = -\mathbf{h}_{\text{alt}} \cdot \sum_i (-1)^i \mathbf{S}_i. \quad (5)$$

The length of the vector \mathbf{h} is given as usual by $g\mu_B B$.

B. Schwinger boson representation

Introduced by Schwinger in 1952 [22], this representation uses two boson flavors $a_i^{(\dagger)}$ and $b_i^{(\dagger)}$ at site i to transform the spin operators as follows

$$S_i^+ = a_i^\dagger b_i, \quad (6a)$$

$$S_i^- = b_i^\dagger a_i, \quad (6b)$$

$$S_i^z = \frac{1}{2} (a_i^\dagger a_i - b_i^\dagger b_i), \quad (6c)$$

so that the spin commutations relations are reproduced. In contrast to the Holstein-Primakoff [19] and Dyson-Maleev bosons [20, 21], both flavors of Schwinger bosons act on any lattice site and are not restricted to one sublattice. The physical meaning of the bosons can be explained best by taking a closer look at the expectation value

$$\langle S_i^z \rangle = \frac{1}{2} \left(\langle a_i^\dagger a_i \rangle - \langle b_i^\dagger b_i \rangle \right). \quad (7)$$

This corresponds to the difference between the mean occupation of the a -bosons and b -bosons at lattice site i . The expectation value $\langle S_i^z \rangle$ is maximized if there are only a -bosons at that lattice site and it is minimized if there are only b -bosons. Expectation values lying between these two extremes are obtained by a mixture or a superposition of the two boson flavors. Given the finite value of the spin length S , it is obvious that the number of bosons per lattice site cannot be arbitrary since the expectation value of a spin along one axis can never be larger than S : $|\langle S_i^z \rangle| \leq S$. To guarantee that only the

physical subspace is considered, $S_i^2 = S(S+1)$ must hold. This condition is equivalent to a local constraint on the number of bosons per lattice site, namely

$$a_i^\dagger a_i + b_i^\dagger b_i = 2S \quad \forall i \in \mathbb{N} \leq N. \quad (8)$$

In the mean-field approach, we refrain from fulfilling this constraint at each site. Instead, we include the constraint in the Hamiltonian as a Lagrange multiplier to ensure (8) on average. By creating a boson of one flavor and annihilating a boson of the other flavor, the ladder operators S^\pm in Eqs. (6a) and (6b) realize transitions between the eigenstates of different magnetic quantum numbers.

Using the Schwinger representation (6), the anisotropic antiferromagnetic Hamiltonian (2b) reads

$$\begin{aligned} \mathcal{H} = J \sum_{\langle i,j \rangle} & \left\{ \frac{\chi}{2} \left(a_i^\dagger b_i b_j^\dagger a_j + a_j^\dagger b_j b_i^\dagger a_i \right) \right. \\ & \left. + \frac{1}{4} \left(a_i^\dagger a_i - b_i^\dagger b_i \right) \left(a_j^\dagger a_j - b_j^\dagger b_j \right) \right\} \end{aligned} \quad (9a)$$

$$\begin{aligned} = J \sum_{\langle i,j \rangle} & \left\{ \frac{\chi}{2} \left(a_i^\dagger b_i b_j^\dagger a_j + a_j^\dagger b_j b_i^\dagger a_i \right) + \right. \\ & \left. \frac{1}{4} \left(a_i^\dagger a_i a_j^\dagger a_j - a_i^\dagger a_i b_j^\dagger b_j - b_i^\dagger b_i a_j^\dagger a_j + b_i^\dagger b_i b_j^\dagger b_j \right) \right\}. \end{aligned} \quad (9b)$$

The model can be extended to M flavors of the Schwinger bosons allowing for an $SU(M)$ symmetry [18, 27, 28]. In this work, however, we stick to two boson flavors a and b since we deal with a spin Hamiltonian with $SU(2)$ -symmetry.

III. MEAN-FIELD THEORY OF THE EQUILIBRIUM

Here we review the equilibrium solutions for the isotropic and the anisotropic cases for three reasons: (i) to introduce the notation, (ii) to discuss the subtleties of the Schwinger boson description, and (iii) to provide the initial conditions for the magnetization switching considered in the following section.

A. Spin isotropic case

By setting $\chi = 1$, the isotropic Schwinger Hamiltonian is obtained from (9b)

$$\begin{aligned} \mathcal{H} = \sum_{\langle i,j \rangle} & \left\{ \frac{1}{2} \left(a_i^\dagger b_i b_j^\dagger a_j + a_j^\dagger b_j b_i^\dagger a_i \right) + \right. \\ & \left. \frac{1}{4} \left(a_i^\dagger a_i a_j^\dagger a_j - a_i^\dagger a_i b_j^\dagger b_j - b_i^\dagger b_i a_j^\dagger a_j + b_i^\dagger b_i b_j^\dagger b_j \right) \right\}. \end{aligned} \quad (10)$$

We use the coupling constant J as the energy unit so that we can set it to unity. Defining the antiferromagnetic

bond operator $A_{ij} := a_i b_j - a_j b_i$, the Hamiltonian can be rewritten to

$$\mathcal{H} = -\frac{1}{2} \sum_{\langle i,j \rangle} \left(A_{ij}^\dagger A_{ij} - 2S^2 \right), \quad (11)$$

where the constraint (8) was used. It is useful to rotate one sublattice by 180° to obtain a uniform description of all lattice sites with full translational invariance. When rotating around the S^y -axis, the x - and z -components of the spin operators change their signs. Consequently, in terms of Schwinger bosons, the substitution

$$a_j \rightarrow -b_j, \quad b_j \rightarrow a_j \quad (12)$$

is applied to one sublattice. The bond operator now reads

$$A_{ij} = a_i a_j + b_i b_j \quad (13)$$

while the representation of the Hamiltonian (11) remains unaltered. Defining the expectation value

$$A := \langle A_{ij} \rangle = \langle A_{ij}^\dagger \rangle \quad (14)$$

and replacing the quadrilinear terms by the terms with one or two contractions according to Wick's theorem the Hamiltonian (11) is converted to the mean-field Hamiltonian

$$\begin{aligned} \mathcal{H} = E_{\text{MF}} + \lambda \sum_i & \left(a_i^\dagger a_i + b_i^\dagger b_i \right) - \\ & \frac{1}{2} A \sum_{\langle i,j \rangle} \left(a_i a_j + b_i b_j + \text{h.c.} \right) \end{aligned} \quad (15)$$

with the mean-field energy $E_{\text{MF}} := N(A^2 + 2S^2)$. Furthermore, to ensure that the constraint (8) is always fulfilled on average, an additional sum with the Lagrange multiplier λ is added.

Calculating the Fourier transformation of the Hamiltonian is the first step towards diagonalization yielding

$$\begin{aligned} \mathcal{H} = E_{\text{MF}} + \sum_{\mathbf{k}} & \left\{ \lambda \left(a_{\mathbf{k}}^\dagger a_{\mathbf{k}} + b_{\mathbf{k}}^\dagger b_{\mathbf{k}} \right) - \right. \\ & \left. A \gamma_{\mathbf{k}} \left(a_{\mathbf{k}} a_{-\mathbf{k}} + b_{\mathbf{k}} b_{-\mathbf{k}} + \text{h.c.} \right) \right\} \end{aligned} \quad (16)$$

with $\gamma_{\mathbf{k}} := \frac{1}{2} (\cos(k_x) + \cos(k_y))$ where we set the lattice constant to unity. Note that the sum refers to the entire Brillouin zone since the Schwinger bosons are not restricted to one sublattice. Next, standard Bogoliubov transformations for both the a - and b -bosons

$$a_{\mathbf{k}}^\dagger = \cosh(\theta_{\mathbf{k}}) \alpha_{\mathbf{k}}^\dagger + \sinh(\theta_{\mathbf{k}}) \alpha_{-\mathbf{k}}, \quad (17a)$$

$$b_{\mathbf{k}}^\dagger = \cosh(\theta_{\mathbf{k}}) \beta_{\mathbf{k}}^\dagger + \sinh(\theta_{\mathbf{k}}) \beta_{-\mathbf{k}}, \quad (17b)$$

and the corresponding Hermitian conjugate relations lead to the diagonalized Hamiltonian

$$\mathcal{H} = E_{\text{MF}} - N\lambda + \sum_{\mathbf{k}} \omega_{\mathbf{k}}^{\text{iso}} \left(\alpha_{\mathbf{k}}^\dagger \alpha_{\mathbf{k}} + \beta_{\mathbf{k}}^\dagger \beta_{\mathbf{k}} + 1 \right), \quad (18)$$

where we have chosen $\lambda \tanh(2\theta_{\mathbf{k}}) = 2A\gamma_{\mathbf{k}}$. The resulting dispersion reads

$$\omega_{\mathbf{k}}^{\text{iso}} = \sqrt{\lambda^2 - (2A\gamma_{\mathbf{k}})^2}. \quad (19)$$

The value λ results from the condition that (8) holds on average, i.e., for the expectation values of the particle numbers. The expectation value A is defined in (14) yielding

$$A = \frac{1}{N} \sum_{\mathbf{k}} \frac{2A\gamma_{\mathbf{k}}^2}{\omega_{\mathbf{k}}^{\text{iso}}} \coth(\beta\omega_{\mathbf{k}}^{\text{iso}}/2), \quad (20a)$$

$$2S + 1 = \frac{1}{N} \sum_{\mathbf{k}} \frac{\lambda}{\omega_{\mathbf{k}}^{\text{iso}}} \coth(\beta\omega_{\mathbf{k}}^{\text{iso}}/2). \quad (20b)$$

Here, β is the inverse temperature up to Boltzmann's constant. Solving these equations requires finding a non-linear zero depending on two variables. For finite systems $N < \infty$ or for finite temperature it can be tackled by direct numerics. No finite sublattice magnetization occurs because no finite system displays long-range anti-ferromagnetic order. The same holds true for the infinite two-dimensional isotropic system at finite temperature according to the Mermin-Wagner theorem [29].

But we briefly discuss the subtle occurrence of long-range order in the infinite system at zero temperature in accordance with previous treatments [18, 23, 24]. The Goldstone theorem [18] tells us that in case of long-range order, the spectrum must be gapless, thus $\lambda = A$ holds. But then we encounter singularities at $\mathbf{k} = \mathbf{0}$ and $\mathbf{k} = (\pi, \pi)$ for finite N . In the thermodynamic limit $N \rightarrow \infty$, the sums in (20) do not converge uniformly to integrals. The solution to this issue lies in the fact that for any finite N the spectrum is *not* gapless, but displays a small finite-size gap Δ_N . Although this gap vanishes for $N \rightarrow \infty$ a contribution from the points $\mathbf{k} = \mathbf{0}$ and $\mathbf{k} = (\pi, \pi)$ remains. Concretely, we set $\lambda^2 = (2A)^2(1 + \kappa^2)$ with $\kappa = f/N$ implying $\omega_{\mathbf{k}}^{\text{iso}} = 2A\sqrt{1 + \kappa^2 - \gamma_{\mathbf{k}}^2}$. Then the limit $N \rightarrow \infty$ is performed for the Eqs. (20) and we obtain

$$A = \frac{1}{4\pi^2} \int_{\text{BZ}} dk^2 \frac{\gamma_{\mathbf{k}}^2}{\sqrt{1 - \gamma_{\mathbf{k}}^2}} + \frac{2}{f}, \quad (21a)$$

$$2S + 1 = \frac{1}{4\pi^2} \int_{\text{BZ}} dk^2 \frac{1}{\sqrt{1 - \gamma_{\mathbf{k}}^2}} + \frac{2}{f}. \quad (21b)$$

This contribution from single points in the Brillouin zone stands for the macroscopic contribution of a few modes, here precisely four modes ($\alpha_{\mathbf{k}}, \beta_{\mathbf{k}}$ at $\mathbf{k} = \mathbf{0}$ and (π, π)), representing a Bose-Einstein condensation. It is directly linked to the occurrence of long-range order because one can show, see Appendix A, that the sublattice magnetization per site $m_0 = |\langle S_i^z \rangle|$ in the ordered phase is given by

$$m_0 = 1/f \quad (22a)$$

$$= S + \frac{1}{2} - \frac{1}{8\pi^2} \int_{\text{BZ}} dk^2 \frac{1}{\sqrt{1 - \gamma_{\mathbf{k}}^2}}. \quad (22b)$$

Subtracting the two equations (21) yields

$$2S + 1 - A = \frac{1}{4\pi^2} \int_{\text{BZ}} dk^2 \sqrt{1 - \gamma_{\mathbf{k}}^2} =: 2\delta + 1 \quad (23a)$$

$$\Leftrightarrow A = 2(S - \delta), \quad (23b)$$

$$2\delta = -0.15795, \quad (23c)$$

$$\omega_{\mathbf{k}}^{\text{iso}} = 4(S - \delta)\sqrt{1 - \gamma_{\mathbf{k}}^2}, \quad (23d)$$

where we determined 2δ numerically.

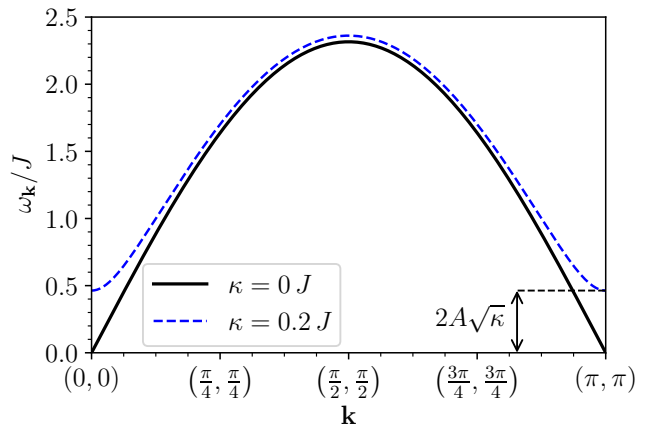


FIG. 1. The black line depicts the degenerate dispersion of the two Schwinger bosons in the long-range ordered isotropic case in the thermodynamic limit. The blue dashed line illustrates the dispersion assuming a finite $\kappa = 0.2J$.

In Fig. 1, we show the resulting dispersion in the thermodynamic limit (black line) and for an arbitrary finite $\kappa = 0.2J$ (blue dashed line) for illustration. Note that the black line shows the dispersion of both the α - and the β -bosons because they are degenerate. Since the spin operators consist of bilinear bosonic expressions, see Eq. (6), a physical excitation, i.e., the magnon, will not consist of a single α or β particle. Given, however, the macroscopic occupations at $\mathbf{k} = \mathbf{0}$ and (π, π) it is justified to replace the bosonic operators at these wave vectors according to

$$\alpha_{\mathbf{k}} \rightarrow \langle \alpha_{\mathbf{k}} \rangle = \sqrt{Nm_0/4}, \quad (24a)$$

$$\beta_{\mathbf{k}} \rightarrow \langle \beta_{\mathbf{k}} \rangle = \sqrt{Nm_0/4} \quad (24b)$$

if no spontaneous symmetry breaking is accounted for. In the ordered phase, only one of the bosons displays the macroscopic occupation, see Appendix A, so that either $\alpha_{\mathbf{k}} \rightarrow \sqrt{Nm_0/2}$ or $\beta_{\mathbf{k}} \rightarrow \sqrt{Nm_0/2}$ holds at $\mathbf{k} = \mathbf{0}$ and (π, π) , see Ref. [18]. With these substitutions the creation of a magnon is described by $\sqrt{Nm_0/2}\beta_{\mathbf{k}}^\dagger$ if the α -bosons condense and by $\sqrt{Nm_0/2}\alpha_{\mathbf{k}}^\dagger$ if the β bosons condense. It is interesting to note that the dispersion from the Schwinger boson mean-field theory is identical to the self-consistent spin-wave theory resulting from a $1/S$ expansion in the Holstein-Primakoff and in the

Dyson-Maleev representation up to and including order $1/S$.

Later we compute solutions for the self-consistency conditions numerically for finite clusters with $N < \infty$ because we need them as initial conditions for switching processes. Rigorously, no spontaneous symmetry breaking takes place due to the finiteness of the sample size and thus no finite sublattice magnetization can be determined. As a remedy to approximate the thermodynamic, infinite lattice, we include a tiny symmetry-breaking alternating field h_{alt}^z . It turns out that a scaling of this auxiliary field has to be chosen $\propto 1/N$. Then it reproduces the analytically known sublattice magnetization $m_0 = S - 0.19660$. The details of the calculation are given in Appendices A and B.

B. Spin anisotropic case

Here we address the anisotropic case and its description by a Schwinger boson mean field theory. This case is more involved since the equations are less symmetric which requires to account for additional mean fields, see for instance Ref. [30]. Conceptually, however, there is an explicit difference in the anisotropic case between the two bosons so that no infinitesimal fields are needed.

By using the constraint (8), the anisotropic Hamiltonian of the antiferromagnetic spin lattice (9b) can be written as

$$\mathcal{H} = -\frac{1}{4} \sum_{\langle i,j \rangle} \left\{ (1+\chi) A_{ij}^\dagger A_{ij} + (1-\chi) B_{ij}^\dagger B_{ij} - 4S^2 \right\} \quad (25)$$

with the bond operators $A_{ij} := a_i a_j + b_i b_j$ and $B_{ij} := a_i a_j - b_i b_j$. As before, one sublattice has been rotated by 180° using the substitution (12) so that all spins point in the same direction in the ordered phase. The mean-field Hamiltonian is obtained by applying Wick's theorem neglecting quadrilinear normal-ordered terms yielding

$$\begin{aligned} \mathcal{H} = & E_{\text{MF}} + \lambda \sum_i \left(a_i^\dagger a_i + b_i^\dagger b_i \right) - \\ & \frac{1}{4} \sum_{\langle i,j \rangle} \left\{ A(1+\chi)(a_i a_j + b_i b_j + \text{h.c.}) + \right. \\ & \left. B(1-\chi)(a_i a_j - b_i b_j + \text{h.c.}) \right\}, \quad (26a) \end{aligned}$$

with $E_{\text{MF}} := \frac{1}{2}N \{A^2(1+\chi) + B^2(1-\chi) + 4S^2\}$ and the expectation values $A := \langle A_{ij} \rangle = \langle A_{ij}^\dagger \rangle$ and $B := \langle B_{ij} \rangle = \langle B_{ij}^\dagger \rangle$.

Furthermore, a boson number term with the Lagrange multiplier λ is added to ensure that the constraint (8) is also satisfied in the anisotropic case on average. With vanishing anisotropy $\chi \rightarrow 1$, this Hamiltonian corresponds to that of the isotropic system (15).

In order to diagonalize the anisotropic Hamiltonian, we proceed as in the isotropic case. After Fourier trans-

formation, the Hamiltonian is given by

$$\begin{aligned} \mathcal{H} = & E_{\text{MF}} + \lambda \sum_{\mathbf{k}} \left(a_{\mathbf{k}}^\dagger a_{\mathbf{k}} + b_{\mathbf{k}}^\dagger b_{\mathbf{k}} \right) \\ & - \frac{1}{2} \sum_{\mathbf{k}} \gamma_{\mathbf{k}} \left\{ A(1+\chi)(a_{\mathbf{k}} a_{-\mathbf{k}} + b_{\mathbf{k}} b_{-\mathbf{k}} + \text{h.c.}) \right. \\ & \left. + B(1-\chi)(a_{\mathbf{k}} a_{-\mathbf{k}} - b_{\mathbf{k}} b_{-\mathbf{k}} + \text{h.c.}) \right\}. \quad (27) \end{aligned}$$

Since the non-diagonal Bogoliubov terms of the two Schwinger bosons flavors have different prefactors, it is no longer possible to use the same Bogoliubov angles in the transformations. Thus we use

$$a_{\mathbf{k}}^\dagger = \cosh(\theta_{\mathbf{k}}^a) \alpha_{\mathbf{k}}^\dagger + \sinh(\theta_{\mathbf{k}}^a) \alpha_{-\mathbf{k}}, \quad (28a)$$

$$b_{\mathbf{k}}^\dagger = \cosh(\theta_{\mathbf{k}}^b) \beta_{\mathbf{k}}^\dagger + \sinh(\theta_{\mathbf{k}}^b) \beta_{-\mathbf{k}}, \quad (28b)$$

and the Hermitian conjugate operators using the condition

$$\gamma_{\mathbf{k}} = \frac{\lambda}{C_-} \tanh(2\theta_{\mathbf{k}}^a) = \frac{\lambda}{C_+} \tanh(2\theta_{\mathbf{k}}^b) \quad (29)$$

with

$$C_{\pm} := (A(1+\chi) \mp B(1-\chi)). \quad (30)$$

In this way, we obtain the diagonal form

$$\mathcal{H} = E_{\text{MF}} - N\lambda + \sum_{\mathbf{k}} \left\{ \omega_{\mathbf{k}}^- \left(\alpha_{\mathbf{k}}^\dagger \alpha_{\mathbf{k}} + \frac{1}{2} \right) + \omega_{\mathbf{k}}^+ \left(\beta_{\mathbf{k}}^\dagger \beta_{\mathbf{k}} + \frac{1}{2} \right) \right\}. \quad (31)$$

Concomitantly, there are two different spin-wave dispersions

$$\omega_{\mathbf{k}}^{\pm} = \sqrt{\lambda^2 - C_{\pm}^2 \gamma_{\mathbf{k}}^2}. \quad (32)$$

For $\chi = 1$, the two dispersions coincide and reproduce the isotropic dispersion (19).

Physically, a spin gap is expected to result from the anisotropy reducing the continuous symmetry to a discrete \mathbb{Z}_2 -symmetry. Therefore, spontaneous symmetry breaking due to the magnetic order no longer breaks a continuous symmetry and no massless Goldstone bosons need to occur. Still, the Schwinger boson description of the ordered phase requires a condensation of one Schwinger boson flavor at zero temperature. Let us assume that the α -bosons condense so that their dispersion is gapless in the thermodynamic limit at $T = 0$. We stress that this does not imply that the physical excitations are gapless because they imply the annihilation of an α -boson combined with the creation of a β -boson.

After these qualitative considerations, we need to derive the conditions for the parameters A , B , and λ in order to be able to make any quantitative statements. The constraint and the expectation values A and B yield

$$2S = \frac{\lambda}{2N} \sum_{\mathbf{k}} \left[\frac{\coth\left(\frac{\beta\omega_{\mathbf{k}}^-}{2}\right)}{\omega_{\mathbf{k}}^-} + \frac{\coth\left(\frac{\beta\omega_{\mathbf{k}}^+}{2}\right)}{\omega_{\mathbf{k}}^+} \right] - 1, \quad (33a)$$

$$A = \frac{1}{2N} \sum_{\mathbf{k}} \gamma_{\mathbf{k}}^2 \left[\frac{C_- \coth\left(\frac{\beta\omega_{\mathbf{k}}^-}{2}\right)}{\omega_{\mathbf{k}}^-} + \frac{C_+ \coth\left(\frac{\beta\omega_{\mathbf{k}}^+}{2}\right)}{\omega_{\mathbf{k}}^+} \right], \quad (33b)$$

$$B = \frac{1}{2N} \sum_{\mathbf{k}} \gamma_{\mathbf{k}}^2 \left[\frac{C_- \coth\left(\frac{\beta\omega_{\mathbf{k}}^-}{2}\right)}{\omega_{\mathbf{k}}^-} - \frac{C_+ \coth\left(\frac{\beta\omega_{\mathbf{k}}^+}{2}\right)}{\omega_{\mathbf{k}}^+} \right]. \quad (33c)$$

These equations allow us to determine the dispersion at zero and finite temperature. The case of zero temperature is again a bit subtle; the relevant treatment of the equations at $T = 0$ is described in Appendix C. The resulting dispersion is displayed in Fig. 2. Clearly the spin gap in the physical dispersion appears and grows for larger anisotropy.

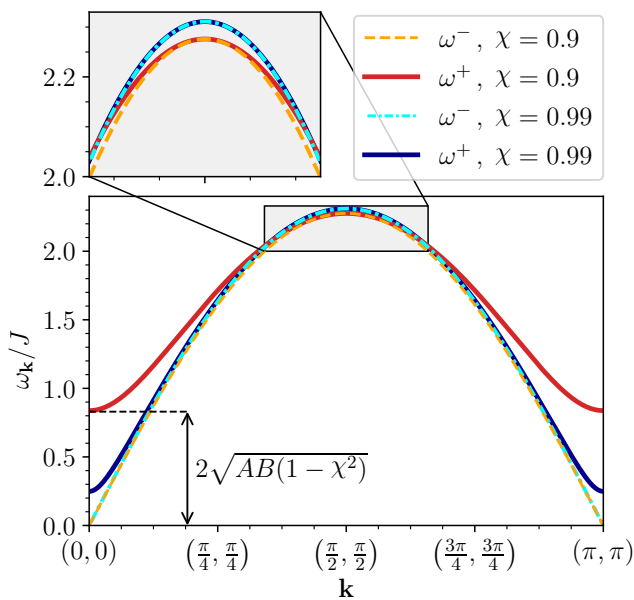


FIG. 2. Dispersions $\omega_{\mathbf{k}}^{\pm}$ in an antiferromagnetic spin- $\frac{1}{2}$ square lattice at zero temperature, plotted exemplarily for the two anisotropies $\chi = 0.9$ and $\chi = 0.99$. For the same χ , the maxima of the dispersions $\omega_{\mathbf{k}}^+$ and $\omega_{\mathbf{k}}^-$ coincide, while $\omega_{\mathbf{k}}^-$ is gapless and $\omega_{\mathbf{k}}^+$ displays the physical energy gap at $\mathbf{k} = (0, 0)$ and $\mathbf{k} = (\pi, \pi)$. Note that $\omega_{\mathbf{k}}^-$ does not describe observable modes. As expected, the energy gap $\Delta = 2\sqrt{AB(1-\chi^2)}$ increases with increasing anisotropy, i.e., increasing deviation of χ from 1.

The behavior of the spin gap Δ as function of the anisotropy parameter χ is of particular interest. The required input parameter is the product AB . The behavior of A , B and of their product is shown in Fig. 19 in Appendix C. The expectation value A appears to be

smooth while B and thus the product AB display a singular behavior at $\chi = 1$. Figure 3 depicts the spin gap and compares it with recently published data obtained by a different advanced semi-analytical approach using continuous similarity transformations (CST) [31]. The latter can be considered to be reliable. Good agreement is obtained if the CST data is rescaled by the factor 1.3. In view of the simplicity of the mean-field approach, this agreement is satisfactory. In particular, mean-field and CST results are consistent with a square root behavior $\Delta \propto (1-\chi^2)^{\mu}$ even though fitting indicates slightly larger exponents $\mu \approx 0.54$.

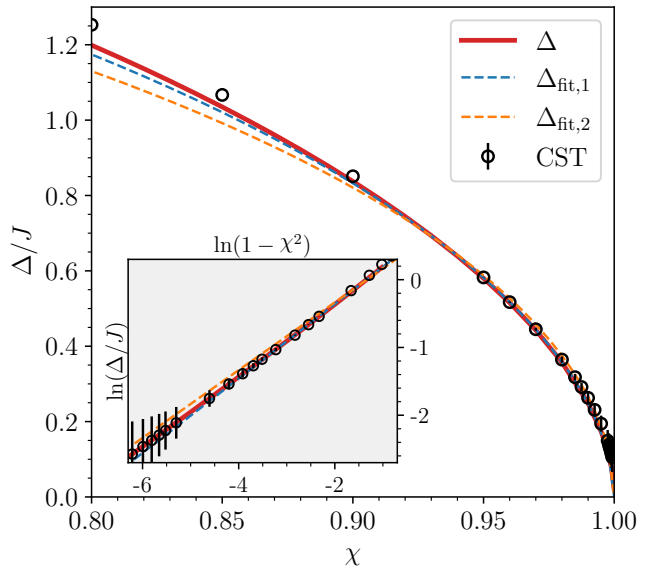


FIG. 3. The spin gap Δ plotted as a function of the anisotropy χ . The red solid curve shows the Schwinger boson mean-field data while the dashed curves are fits: $\Delta_{\text{fit},i} = c_i(1-\chi^2)^{\mu_i}$ in blue with $c_1 = (2.04 \pm 0.06)J$, $\mu_1 = 0.54 \pm 0.02$ and the orange curve with $\mu_2 = 1/2$ and $c_2 = (1.88 \pm 0.06)J$. The black symbols represent gap values obtained by CST [31] rescaled by the factor 1.3.

In order to determine the magnetization we rewrite Eq. (7) in terms of the α - and β -particles and explicitly obtain

$$m_0 = \frac{\lambda}{2N} \sum_{\mathbf{k}} \left[\frac{\coth\left(\frac{\beta\omega_{\mathbf{k}}^-}{2}\right)}{\omega_{\mathbf{k}}^-} - \frac{\coth\left(\frac{\beta\omega_{\mathbf{k}}^+}{2}\right)}{\omega_{\mathbf{k}}^+} \right]. \quad (34)$$

Its evaluation at $T = 0$ is given in Appendix C yielding

$$m_0 = S + \frac{1}{2} - \frac{1}{8\pi^2} \int_{\text{BZ}} dk^2 \frac{C_-}{\sqrt{C_-^2 - C_+^2 \gamma_{\mathbf{k}}^2}}. \quad (35)$$

The explicit data is displayed in Fig. 4 as function of χ for $S = 1/2$. As expected the magnetization approaches its maximum value S for $\chi \rightarrow 0$ where the model becomes the Ising model.

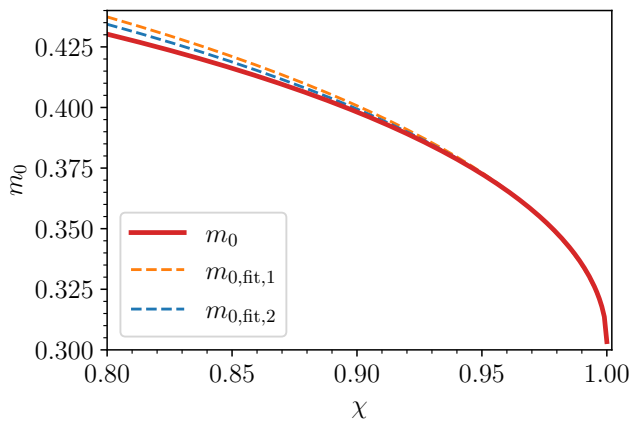


FIG. 4. The magnetization at zero temperature is shown as function of the anisotropy parameter χ according to Eq. (35) as solid red line. The fit functions are $m_{0,\text{fit},i} = m_{0,\text{iso}} + c_i(1 - \chi^2)_i^{\mu_i}$ in blue with $c_1 = (0.215 \pm 0.005)J$, $\mu_1 = 0.49 \pm 0.01$ and the orange curve with $\mu_2 = 1/2$ and $c_2 = (0.223 \pm 0.004)J$.

C. Finite temperature

Here we turn to the effect of finite temperature. We are not interested in the phase without order occurring at high temperatures above the Néel temperature T_N . In the ordered phase, a difference between the dispersion of the α -boson and the β -boson persists. In contrast, however, to zero temperature no condensation of either boson occurs. Both bosons become gapped at finite temperature. Note that this does not imply that there is no longer a finite sublattice magnetization m_0 because the anisotropy ensures that $m_0 \neq 0$ is possible also up to some finite Néel temperature.

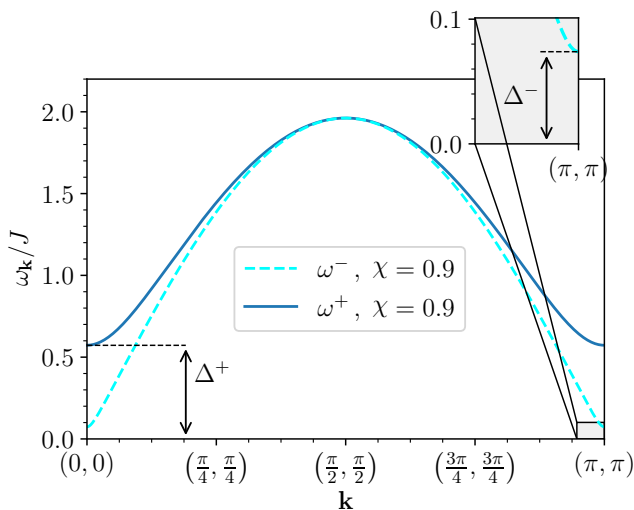


FIG. 5. Dispersions $\omega_{\mathbf{k}}^{\pm}$ in an antiferromagnetic spin- $\frac{1}{2}$ square lattice at finite temperature, plotted exemplarily for $\chi = 0.9$ at $T = 0.65J$.

For simplicity and for later use we consider a finite mesh of the Brillouin zone on which we evaluate the expectation values required to determine A , B , and the Lagrange parameter λ self-consistently, see also Sect. IV. This is done for systems with linear extension up to $L = 200$ at finite temperature and up to $L = 500$ at zero temperature so that finite size effects are very small and negligible. In order to find the self-consistent solution of the ordered phase in practical implementations one must start from initial guesses for the parameters which allow for a difference between the α - and the β -boson. This means one has to start with some finite $B > 0$.

Fig. 5 displays the resulting dispersions $\omega_{\mathbf{k}}^-$ of the α -boson and $\omega_{\mathbf{k}}^+$ of the β -boson. As stated before, both are gapped. But for positive m_0 the dispersion $\omega_{\mathbf{k}}^-$ is still lower than the dispersion $\omega_{\mathbf{k}}^+$ so that more a -bosons are present than b -bosons. We define the gaps

$$\Delta^{\pm} := \omega_{\mathbf{k}=\mathbf{0}}^{\pm}, \quad (36a)$$

$$\Delta := \Delta^+ - \Delta^-. \quad (36b)$$

The gaps Δ^{\pm} are auxiliary quantities without direct physical meaning because the physical spin excitations always imply an action on two bosons. In particular, the annihilation of an α -boson and the creation of a β -boson represents a spin flip down for $S = 1/2$ or generally a lowering of the sublattice magnetization by the creation of one magnon. Thus, the above quantity Δ represents the physical spin gap. Figure 6 displays the auxiliary gaps Δ^{\pm} in panel (a) and the physical gap Δ in panel (b). In a rigorous treatment, the spin gap is a property at $T = 0$ referring to the minimum energy between the ground state and the first excited state(s). In this view, no “temperature dependent” spin gap makes sense. The spin gap in a mean-field theory must be seen as an *effective* spin gap which reflects the gap of the bilinear mean-field Hamiltonian which describes the physics of the underlying interacting model best at a given temperature.

Once we know all the expectation values in reciprocal space we also know all expectation values in real space. Thus the sublattice magnetization can also be computed and it is displayed as function of temperature in Fig. 7 up to the respective Néel temperatures. The power law close to the Néel temperatures is expected to be a square root law as is generic for mean-field theories. Our data is fully consistent with this assumption. The analogous square root law is consistent with our findings for the effective spin gap Δ in Fig. 6(b).

Finally, Fig. 8 depicts the Néel temperature as function of the anisotropy according to the Schwinger boson mean-field theory. As pointed out before this mean-field theory complies with the rigorous Mermin-Wagner theorem [29] so that $\lim_{\chi \rightarrow 1} T_N(\chi) = 0$ holds. But the downturn upon approaching the isotropic case is extremely steep. From the integrals in the derivation of the Mermin-Wagner theorem for two dimensions a logarithmic dependence according to $T_N/J \approx c_1/(|\ln(1 - \chi)| + c_2)$ appears plausible, see caption. To estimate the accuracy of our results

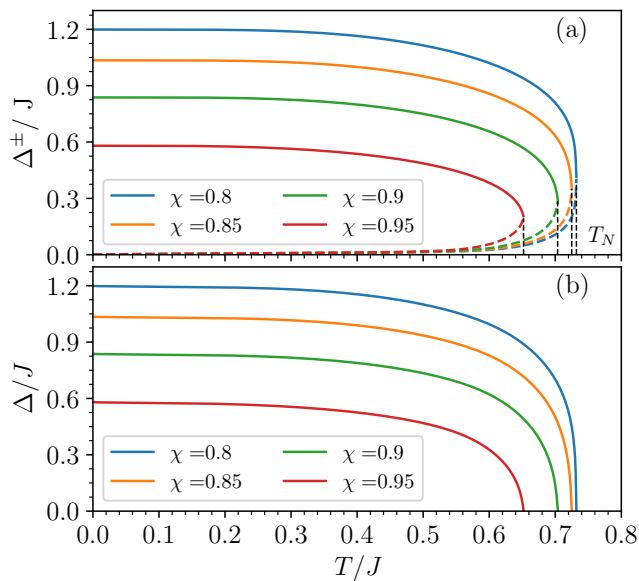


FIG. 6. Panel (a): Auxiliary gaps Δ^\pm as function of temperature for various anisotropies χ . The gap Δ^+ shown by solid lines refers to the β -bosons; the gap Δ^- shown by dashed lines refers to the α -bosons. The two gaps merge at the Néel temperature T_N indicated by short vertical black lines. Panel (b): Effective physical gap Δ according to Eq. (36b).

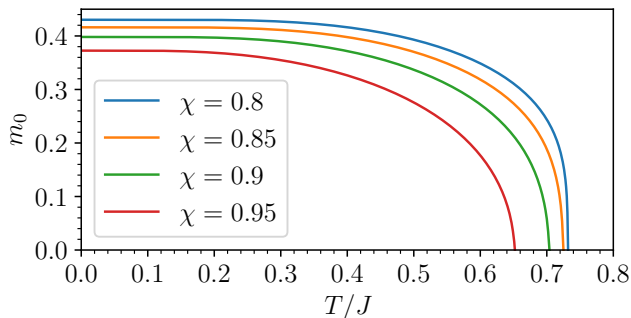


FIG. 7. Sublattice magnetization m_0 as defined in Eq. (7) for various anisotropies χ as function of temperature. The solid line is a guide to the eye. It vanishes at the Néel temperature, where the ordered phase ceases to exist, with a square root behavior.

we can compare them at $\chi = 0$ with the rigorous result of Onsager [32] for the two-dimensional Ising model yielding $T_N = 0.5673J$. As for the gap, the results agree if the mean-field results are scaled down by a factor of 1.3.

The results presented in this section provide an overview of the essential properties of the system in equilibrium. It is crucial to know them quantitatively because they define the initial conditions for the subsequent time-dependent solutions which describe the switching process.

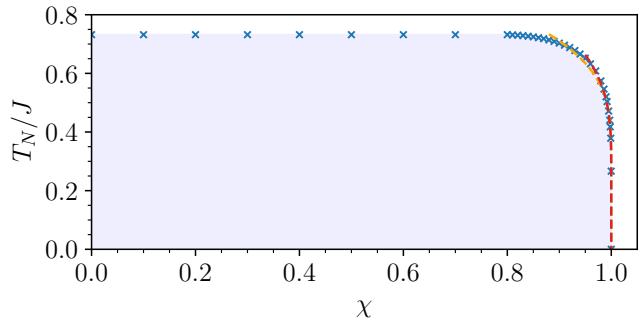


FIG. 8. Néel temperature as function of the anisotropy. In accord with the Mermin-Wagner theorem, the Néel temperature vanishes in the isotropic case, i.e., for $\chi \rightarrow 1$. The vanishing of T_N close to the isotropic point can be fitted according to $T_N/J \approx c_1/(|\ln(1-\chi)| + c_2)$ with $c_1 = 4.1 \pm 0.08$ and $c_2 = 3.5 \pm 0.02$ in the interval $\chi \in [0.88, 1]$ (orange dashed line) and with $c_1 = 3.5 \pm 0.05$ and $c_2 = 2.3 \pm 0.06$ in the interval $\chi \in [0.95, 1]$ (red dashed line).

IV. SWITCHING THE SUBLATTICE MAGNETIZATION

The aim is to invert the sublattice magnetization $m_0 \rightarrow -m_0$. We denote the time-dependent sublattice magnetization during the switching process by $m(t)$. One can think of this process as switching a bit from its 1-state to its 0-state. Hence, the considered process is highly relevant in data storage with the advantages exposed in the Introduction.

We have a precessional rotation in mind. Thus we add a static magnetic field along the S^y -axis in form of a Zeeman term from time $t = 0$ onwards

$$\mathcal{H} = \mathcal{H}_0 - h_y \sum_i S_i^y \quad (37a)$$

$$= \mathcal{H}_0 - \frac{h_y}{2i} \sum_i (S_i^+ - S_i^-) \quad (37b)$$

$$= \mathcal{H}_0 - \frac{h_y}{2i} \sum_i (a_i^\dagger b_i - b_i^\dagger a_i), \quad (37c)$$

where \mathcal{H}_0 is the unperturbed Hamiltonian (15).

For the isotropic case, the Zeeman term does not change under the Bogoliubov transformation yielding

$$\mathcal{H} = E_{\text{MF}} - N\lambda + \sum_{\mathbf{k}} \omega_{\mathbf{k}}^{\text{iso}} \left(\alpha_{\mathbf{k}}^\dagger \alpha_{\mathbf{k}} + \beta_{\mathbf{k}}^\dagger \beta_{\mathbf{k}} + 1 \right) - \frac{h_y}{2i} \sum_{\mathbf{k}} \left(\alpha_{\mathbf{k}}^\dagger \beta_{\mathbf{k}} - \beta_{\mathbf{k}}^\dagger \alpha_{\mathbf{k}} \right). \quad (38)$$

Due to the spin isotropy the Zeeman term commutes with the Hamiltonian so that any ground state of \mathcal{H}_0 remains a ground state under the action of the Zeeman term. The Zeeman term induces a collective rotation about S^y at all sites simultaneously. The rotation of each spin can be treated as if the spin were isolated. Hence, the sublattice

magnetization is rotated in the $S^z S^x$ -plane. A rotation about the angle φ is achieved within the time interval

$$t_\varphi = \frac{\varphi}{h_y}. \quad (39)$$

This can be verified in terms of the spin operators or in terms of the Schwinger bosons. The tilt $m_0 \rightarrow -m_0$ is achieved for $t_\pi = \pi/h_y$. No minimum magnetic field is required to achieve the rotation if one can create long enough pulses of constant magnetic fields. Yet, this case is not promising for application because the absence of any anisotropy also implies that the system does not have any rigidity of the sublattice magnetization against perturbations.

For this reason, we turn to the anisotropic case where the situation is more subtle because the Zeeman term does not commute with the Hamiltonian. We have to compute the time evolution under the full mean-field Hamiltonian

$$\begin{aligned} \mathcal{H} = E_{\text{MF}} - \frac{1}{2} \sum_{\mathbf{k}} \gamma_{\mathbf{k}} & \left(C_- a_{\mathbf{k}}^\dagger a_{-\mathbf{k}}^\dagger + C_+ b_{\mathbf{k}}^\dagger b_{-\mathbf{k}}^\dagger \right. \\ & \left. + C_- a_{\mathbf{k}} a_{-\mathbf{k}} + C_+ b_{\mathbf{k}} b_{-\mathbf{k}} \right) + \lambda \sum_{\mathbf{k}} \left(a_{\mathbf{k}}^\dagger a_{\mathbf{k}} + b_{\mathbf{k}}^\dagger b_{\mathbf{k}} \right) \\ & - \frac{h_y}{2i} \sum_{\mathbf{k}} \left(a_{\mathbf{k}}^\dagger b_{\mathbf{k}} - b_{\mathbf{k}}^\dagger a_{\mathbf{k}} \right). \end{aligned} \quad (40)$$

We stress that the prefactors C_\pm defined in Eq. (30) depend on expectation values which themselves acquire a temporal dependence upon switching. Hence the above Hamiltonian itself is time dependent. We refrain from expressing the Hamiltonian (40) in terms of Bogoliubov particles $\alpha_{\mathbf{k}}$ and $\beta_{\mathbf{k}}$ because no useful simplification can be reached due to the time dependence of the C_\pm . It would require to adjust the Bogoliubov transformation at each instant of time in order to keep diagonality. This is tedious and does not promise neither insight nor advantage.

The Hamiltonian (40) is fully sufficient to compute the time dependence of the expectation values by means of Heisenberg's equations of motion. This amounts up to the density-matrix formalism. The set of differential

equations reads

$$\begin{aligned} \partial_t \langle a_{\mathbf{k}}^\dagger a_{\mathbf{k}} \rangle &= 2\gamma_{\mathbf{k}} \text{Im} \left(C_-^* \langle a_{\mathbf{k}} a_{-\mathbf{k}} \rangle \right) \\ &+ \frac{h_y}{2} \left(\langle a_{\mathbf{k}}^\dagger b_{\mathbf{k}} \rangle + \langle b_{\mathbf{k}}^\dagger a_{\mathbf{k}} \rangle \right), \end{aligned} \quad (41a)$$

$$\begin{aligned} \partial_t \langle b_{\mathbf{k}}^\dagger b_{\mathbf{k}} \rangle &= 2\gamma_{\mathbf{k}} \text{Im} \left(C_+^* \langle b_{\mathbf{k}} b_{-\mathbf{k}} \rangle \right) \\ &- \frac{h_y}{2} \left(\langle a_{\mathbf{k}}^\dagger b_{\mathbf{k}} \rangle + \langle b_{\mathbf{k}}^\dagger a_{\mathbf{k}} \rangle \right), \end{aligned} \quad (41b)$$

$$\begin{aligned} \partial_t \langle a_{\mathbf{k}}^\dagger b_{\mathbf{k}} \rangle &= -i\gamma_{\mathbf{k}} \left(C_-^* \langle a_{\mathbf{k}} b_{-\mathbf{k}} \rangle - C_+ \langle a_{\mathbf{k}}^\dagger b_{-\mathbf{k}}^\dagger \rangle \right) \\ &+ \frac{h_y}{2} \left(\langle b_{\mathbf{k}}^\dagger b_{\mathbf{k}} \rangle - \langle a_{\mathbf{k}}^\dagger a_{\mathbf{k}} \rangle \right), \end{aligned} \quad (41c)$$

$$\begin{aligned} \partial_t \langle a_{\mathbf{k}} a_{-\mathbf{k}} \rangle &= i\gamma_{\mathbf{k}} \left[C_- (2\langle a_{\mathbf{k}}^\dagger a_{\mathbf{k}} \rangle + 1) \right] \\ &- 2\lambda i \langle a_{\mathbf{k}} a_{-\mathbf{k}} \rangle + h_y \langle a_{\mathbf{k}} b_{-\mathbf{k}} \rangle, \end{aligned} \quad (41d)$$

$$\begin{aligned} \partial_t \langle b_{\mathbf{k}} b_{-\mathbf{k}} \rangle &= i\gamma_{\mathbf{k}} \left[C_+ (2\langle b_{\mathbf{k}}^\dagger b_{\mathbf{k}} \rangle + 1) \right] \\ &- 2\lambda i \langle b_{\mathbf{k}} b_{-\mathbf{k}} \rangle - h_y \langle a_{\mathbf{k}} b_{-\mathbf{k}} \rangle, \end{aligned} \quad (41e)$$

$$\begin{aligned} \partial_t \langle a_{\mathbf{k}} b_{-\mathbf{k}} \rangle &= i\gamma_{\mathbf{k}} \left(C_- \langle a_{\mathbf{k}}^\dagger b_{\mathbf{k}} \rangle + C_+ \langle a_{\mathbf{k}}^\dagger b_{\mathbf{k}} \rangle^* \right) - 2\lambda i \langle a_{\mathbf{k}} b_{-\mathbf{k}} \rangle \\ &- \frac{h_y}{2} \left(\langle a_{\mathbf{k}} a_{-\mathbf{k}} \rangle - \langle b_{\mathbf{k}} b_{-\mathbf{k}} \rangle \right). \end{aligned} \quad (41f)$$

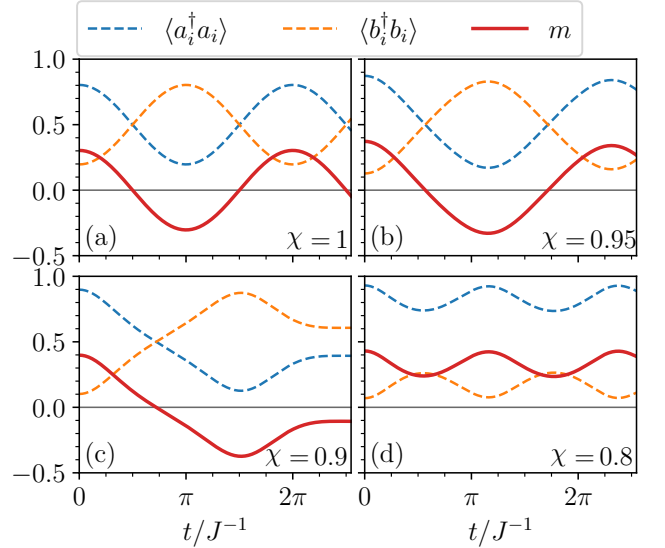


FIG. 9. Dynamics of the occupation of the Schwinger bosons $\langle a_i^\dagger a_i \rangle$ and $\langle b_i^\dagger b_i \rangle$, as well as the resulting magnetization m in the time interval $t \in [0 J^{-1}, 8 J^{-1}]$ for exemplary values of the anisotropy. The strength of the applied field is $h = 1 J$ so that in the isotropic case (panel (a), $\chi = 1$), the switching duration of $t = \pi J^{-1}$ for the π -pulse results in accord with Eq. (39). The calculations were performed for a system size of $L = 500$ implying $N = 250,000$.

In terms of the initial Schwinger bosons without any Bogoliubov transformations, the relations defining $A, B,$

and the constraint read

$$A = \langle a_i a_j \rangle + \langle b_i b_j \rangle = \frac{1}{N} \sum_{\mathbf{k}} \gamma_{\mathbf{k}} (\langle a_{\mathbf{k}} a_{-\mathbf{k}} \rangle + \langle b_{\mathbf{k}} b_{-\mathbf{k}} \rangle), \quad (42a)$$

$$B = \langle a_i a_j \rangle - \langle b_i b_j \rangle = \frac{1}{N} \sum_{\mathbf{k}} \gamma_{\mathbf{k}} (\langle a_{\mathbf{k}} a_{-\mathbf{k}} \rangle - \langle b_{\mathbf{k}} b_{-\mathbf{k}} \rangle), \quad (42b)$$

$$2S = \langle a_i^\dagger a_i \rangle + \langle b_i^\dagger b_i \rangle = \frac{1}{N} \sum_{\mathbf{k}} (\langle a_{\mathbf{k}}^\dagger a_{\mathbf{k}} \rangle + \langle b_{\mathbf{k}}^\dagger b_{\mathbf{k}} \rangle), \quad (42c)$$

where i, j are adjacent sites. This completes a closed set of differential equations. The constraint (42c) is not needed for the temporal equation. But we checked that it is always fulfilled in the course of time if it is fulfilled initially as is ensured by starting from a valid equilibrium solution.

A. Switching at zero temperature

Figure 9 displays the dynamics of the occupations of the Schwinger bosons and the resulting sublattice magnetization $m(t)$ given by

$$m(t) = (\langle a_i^\dagger a_i \rangle - \langle b_i^\dagger b_i \rangle) / 2 = \frac{1}{2N} \sum_{\mathbf{k}} (\langle a_{\mathbf{k}}^\dagger a_{\mathbf{k}} \rangle - \langle b_{\mathbf{k}}^\dagger b_{\mathbf{k}} \rangle) \quad (43)$$

for various values of the anisotropy parameter χ . Panel (a) shows the result for the isotropic case. The external field applied perpendicular to the sublattice magnetization m_0 nicely rotates it following a cosine-curve to $-m_0$ at time t_π predicted by Eq. (39). Since the switching field persists the magnetization is switched back to the initial value at $t = 2t_\pi$. No reduction of m due to dephasing is discernible; the rotation is fully coherent.

Panel (b) reveals differences to the isotropic case. First, the initial magnetization is larger in agreement with the results shown in Fig. 4. The switching to negative values of m succeeds, but it takes longer than in the isotropic case. We attribute this to the anisotropy which hinders the rotation to take place although the state with sublattice magnetization $-m_0$ is also a valid ground state. But the states in between are neither ground states nor eigenstates of the system. This leads to dephasing of the modes at different wave vectors and implies that $|m(t)|$ does not reach the initial value m_0 anymore.

Increasing the anisotropy by lowering χ we see an even longer switching process in panel (c) of Fig. 9. Surprisingly, only one switching appears to be possible since the switching back to the original sign of m does not take place. The switched modes appear to be out of phase, i.e., dephasing has been quite detrimental. We emphasize that such effects are not captured by the description of the sublattice magnetization by a classical vector. Finally, panel (d) displays an example where no switching occurs at all. The sublattice magnetization oscillates

only a little below its initial value m_0 . These observations show that a minimum magnetic field is required in order to change the sign of m . The anisotropy generates a degree of robustness which needs to be overcome by the external magnetic field.

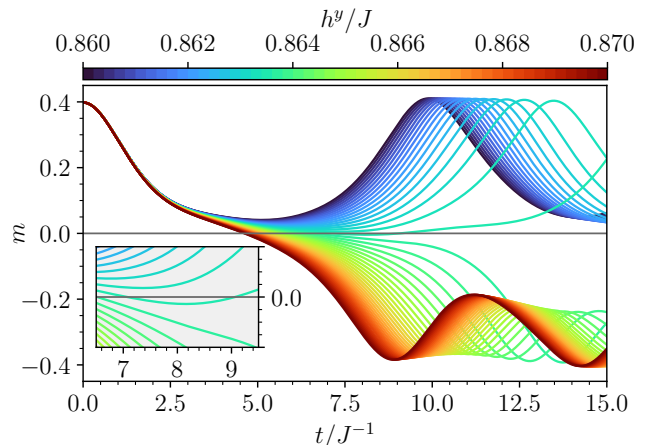


FIG. 10. Time evolution of the magnetization m for various external fields $h^y \in [0.86 J, 0.87 J]$ at the anisotropy $\chi = 0.9$. The color bar on top indicates the external field. Clearly, qualitatively distinct temporal behaviors occur depending on the strength of the applied magnetic field. There is a threshold value h_t above which switching is possible and below which no switching is possible.

In order to further investigate the conditions for successful switching we scan $m(t)$ for a range of applied magnetic fields in Fig. 10. We observe a distinct difference in the behavior for lower fields compared to the behavior for larger ones. Large ones enable switching and low ones do not. There is a well-defined value h_t separating the two regimes. We define a criterion to distinguish whether switching is possible or not. The occurrence of a negative value of $m(t)$ is not an ideal criterion as the inset of Fig. 10 shows. Instead, we choose the occurrence of an inflection point before the first extremal value for $t > 0$ as criterion. If such an inflection point exists $m(t)$ continues to turn down reaching a substantial negative value. Otherwise, no switching is possible.

Next, we quantify how long the switching takes. The duration t is the instant in time when the negative minimum is reached. If no switching is possible, we define the instant in time when the positive maximum is reached as the duration of the failed switching attempt. These durations are plotted in Fig. (11) together with suitable logarithmic fits

$$t_{\text{fit}}(h^y) = c_1 + c_2 \ln |(h^y - h_t)/J|. \quad (44)$$

The fits describe the data remarkably well below and above the threshold with very similar parameters for the

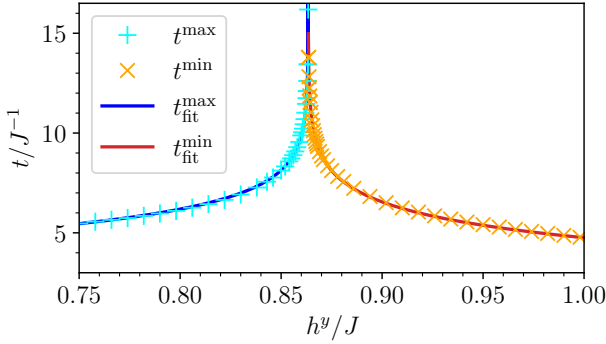


FIG. 11. Times (symbols) at which $m(t)$ reaches the relevant minimum or maximum, depending on whether switching is possible (orange) or not (cyan) plotted against the external field h^y . The position of the singularity defines the threshold field h_t . More data points were computed around the singularity to obtain a higher accuracy for fitting the function given in Eq. (44).

minima (succeeded switching)

$$c_1^{\min} = (2.04 \pm 0.06)J^{-1}, \quad (45a)$$

$$c_2^{\min} = (-1.36 \pm 0.01)J^{-1}, \quad (45b)$$

$$h_t^{\min} = (0.8634 \pm 5 \cdot 10^{-6})J, \quad (45c)$$

and for the maxima (failed switching)

$$c_1^{\max} = (2.73 \pm 0.08)J^{-1}, \quad (46a)$$

$$c_2^{\max} = (-1.25 \pm 0.01)J^{-1}, \quad (46b)$$

$$h_t^{\max} = (0.8634 \pm 6 \cdot 10^{-7})J. \quad (46c)$$

Clearly, the resulting threshold value for $\chi = 0.9$ is $(0.8634 \pm 5 \cdot 10^{-6})J$ which is quite substantial and fairly close to the value of the spin gap Δ . The question suggests itself why such a logarithmic divergence occurs. We argue that this kind of divergence is a clear signature that the magnetic order in antiferromagnets has a certain inertia in its dynamics. This was observed in experiment and supported by a calculation based on classical equations of motion for the antiferromagnetic vector describing the size and direction of the sublattice magnetization [13]. The fact that the microscopic spin-wave description reproduces this behavior corroborates the idea of an inertia of the antiferromagnetic order convincingly. In Appendix D we show that a classical motion of a massive particle over an activation barrier reproduces the logarithmic singularity which we observed. This supports the above interpretation.

We determine these threshold values of a range of anisotropies by bisection with high accuracy. The resulting data is shown in Fig. 12 by the symbols. We compare them with the values of the spin gap shown above in Fig. 3. They are very close to each other for a range of anisotropies. Thus, we conclude that it is the size of the

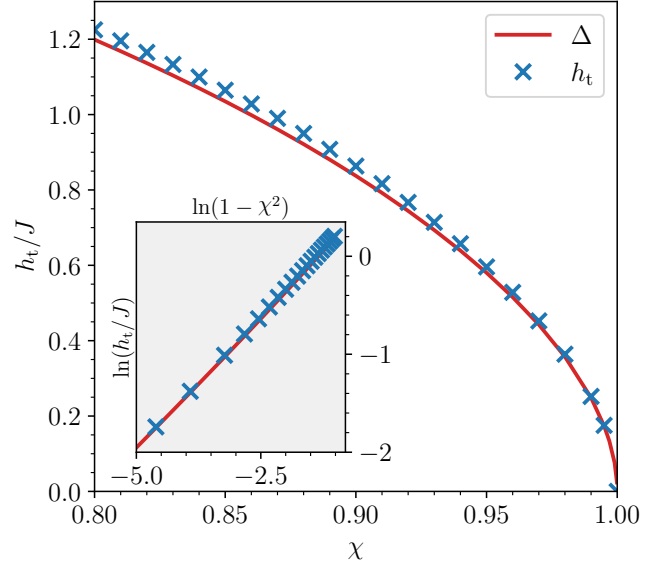


FIG. 12. Threshold magnetic field h_t depicted by the blue symbols vs. anisotropy χ . The data is obtained for a system size $L = 500$. The red solid curve reproduces the spin gap from Fig. 3 to illustrate that the threshold magnetic fields are essentially determined by the size of the spin gap.

spin gap which determines the typical field strength required for switching. This is in line with the idea that the spin gap measures the robustness of the system against any kind of perturbation.

We emphasize that a key aspect of the description of the switching dynamics in terms of spin-waves is that the contribution of each mode is captured individually. The whole process is not one single collective motion, but it consists of the contributions of a thermodynamically large number of modes. Hence, the coherence is not preserved in the course of the switching process except in the isotropic case. This could be inferred already from the decrease of the maximum values of $|m(t)|$ in Fig. 9, i.e., $|m(t)| < m_0$ except for $t = 0$. To underline this aspect further Fig. 13 displays the energy in the course of the switching measured by the expectation value of \mathcal{H}_0

$$E(t) = N \left\{ 2S\lambda + 2S^2 - \langle a_i a_j \rangle \langle a_i^\dagger a_j^\dagger \rangle - \langle b_i b_j \rangle \langle b_i^\dagger b_j^\dagger \rangle - \chi \left(\langle b_i b_j \rangle \langle a_i^\dagger a_j^\dagger \rangle + \langle b_i^\dagger b_j^\dagger \rangle \langle a_i a_j \rangle \right) \right\}. \quad (47)$$

The dynamics of the energy relative to the energy of the initial state $E_0(t) := E(t) - E(0)$ is depicted in Fig. 13 in the time interval $t \in [0, \pi/J]$ for various degrees of anisotropy $\chi \in [0.8, 0.99]$. The magnetic field was chosen relatively high at $h = 2J$ so that a rotation is possible for all anisotropies in the studied range.

As expected, there is an energy minimum after switching since at this instant of time the switched state is closest to the other ground state with magnetization $-m_0$. In the isotropic case $\chi = 1$, the first minimum is reached at the time $t = \pi/(2J)$ according to Eq. (39). However,

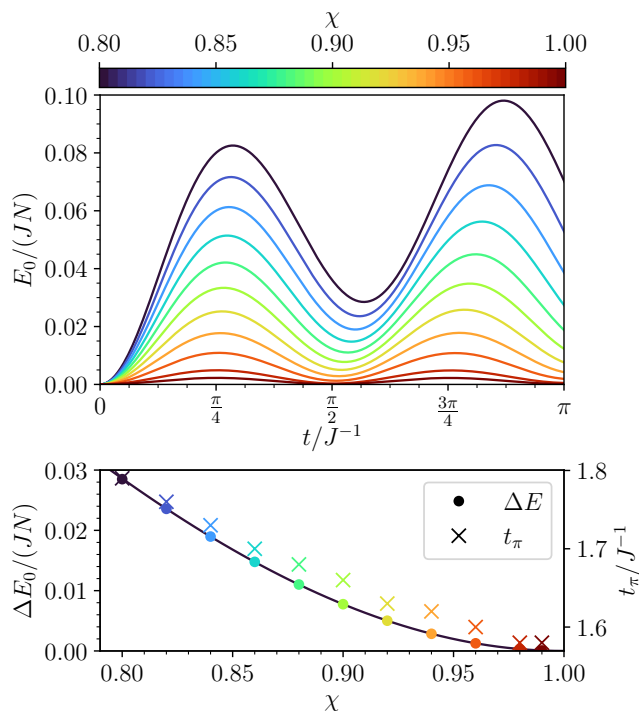


FIG. 13. In the upper panel, the temporal evolution of the energy E_0 per lattice site is shown for an external field $h = 2J$ and various anisotropies $\chi \in [0.8, 0.99]$. The color bar indicates the value of anisotropy. The energy minima ΔE_0 show the energy after switching the magnetization by 180° ; they are not zero but indicate an energy increase because the switching does not lead to the degenerate ground state with magnetization $-m_0$. The energy increase after switching as well as the switching duration t_π are plotted against the anisotropy in the lower panel. The solid line results from a parabolic fit of the energy increase.

as already seen in Fig. 9, the switching duration increases and the minimum shifts to larger times upon increasing anisotropy (lowering of χ). It is obvious that the energy of the initial state is not reached again so that the overall energy is higher after switching the sublattice magnetization for $\chi < 1$. This underlines the effect of the many contributing spin modes which dephase and thereby depart from the initial coherent ground state.

The lower plot in Fig. 13 shows the increase in energy ΔE_0 after switching and the time t_π at which the energy minimum is reached as function of χ . The data points for ΔE_0 can be approximated to high accuracy by a parabola $\Delta E_0(\chi) = c_0(1 - \chi^2)^m$ with the parameters

$$c_0 = (0.230 \pm 0.002)J, \quad (48a)$$

$$m = 2.04 \pm 0.05. \quad (48b)$$

The switching times also increase steadily with growing anisotropy, but they do not evolve completely smoothly in our simulation, especially for $\chi \rightarrow 1$. This is to be attributed to the finite discretization used in the numerical computations.

B. Switching at finite temperature

So far, we studied the conditions for switching the magnetization at zero temperature. But the effect of finite temperature is highly relevant for two reasons. First, having applications in mind, a finite temperature must be accounted for because no setup will be operated at zero temperature. Second, temperature is a parameter which reduces the effective spin gap and makes the ordered system less robust and thus easier to switch. For this reason, a study of finite temperatures is in order.

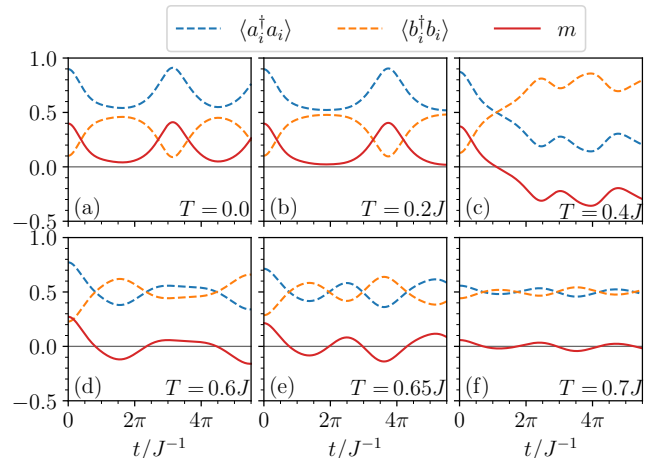


FIG. 14. Same as Fig. 9, but at various temperatures below the Néel temperature $T_N = 0.704J$ for $L = 200$.

Figure 14 shows the effect of finite temperature for an exemplary set of parameters. Clearly, no switching is possible at zero and at low temperatures. But for intermediate temperatures $T \gtrsim 0.4J$, at least one swap $m_0 \rightarrow -m_0$ is possible. Approaching the Néel temperature switching becomes possible even multiple times. Of course, the switched sublattice magnetization is reduced in its absolute value upon approaching T_N . But it can still be manipulated.

This is indeed a very promising observation because it suggests that temporary heating of the system up to the vicinity of the critical temperature, while staying still below it, facilitates the writing process of information into a long-range ordered magnetic system. For long time storage, the temperature can be lowered again after the writing process.

Hence, we investigate the finite temperature case further. Figure 15 displays the temporal evolution of $m(t)$ for various applied magnetic fields for a generic set of anisotropy and temperature. The phenomenology is similar, but not identical to the one at zero temperature, cf. Fig. 10. At zero temperature, the switched curves appear to be mirror images of the non-switched curves flipped around $m = 0$. At finite temperature, it is mostly the first minimum of $m(t)$ which decreases further and further upon increasing the control field h^y . Here, we take

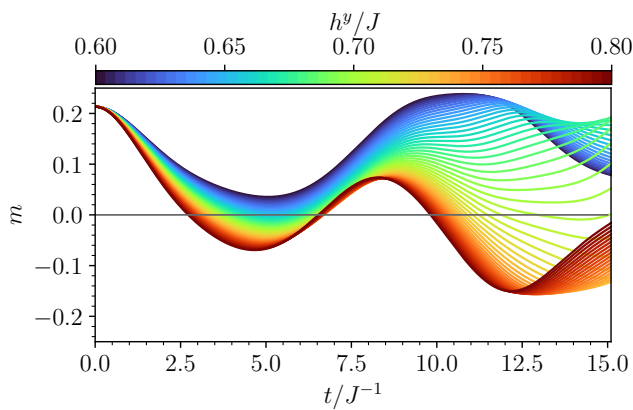


FIG. 15. Time evolution of the magnetization m for various external fields $h^y \in [0.6J, 0.8J]$ at anisotropy $\chi = 0.9$ and temperature $T = 0.65J$ below T_N . The color bar on top indicates the external field. We determine the threshold value h_t from the magnetic field at which the first minimum of $m(t)$ touches $m = 0$.

the occurrence of a negative value of $m(t)$ as signature of switching, i.e., the threshold field h_t is determined from the field at which the first minimum touches the $m = 0$ line. We point out that the threshold field determined in such a way can depend on the considered time interval, see also below, in particular if the instant in time at which the magnetization switches sign jumps as function of the applied field. We analyzed the time interval $t \in [0, 15/h^y]$, i.e., for low values of the field we scanned large intervals. Studying even larger intervals can only lower the values for h_t so that our values are at least rigorous upper bounds.

Next, it is important to track the threshold fields for various temperatures to learn how far they can be reduced by increasing the temperature up to T_N . Since the greatest effects occur close to the Néel temperatures we do not plot the threshold fields as function of T , but as function of the effective spin gap Δ in Fig. 16. We stress that there is a monotonic one-to-one mapping between the temperature and Δ , see Fig. 6(b). Clearly, the data supports the finding that the threshold field h_t decreases reducing the effective spin gap by increasing the temperature to the Néel temperature. But the almost quantitative agreement between threshold field and spin gap we found at zero temperature, see Fig. 12, does not hold anymore. It would have meant that Fig. 16 displayed two straight lines through the origin with identical slope of one. A truly unexpected feature is the discontinuous jump at an intermediate value of the spin gap. It appears to be generic since it occurs for all anisotropies studied. Below the jump only fairly small fields are required to switch the magnetization. For application purposes, we conclude that increasing the temperature close to T_N can help significantly to switch the magnetization. Hence, one may envisage that writing magnetic data is done at elevated temperatures while the long-time storage is done

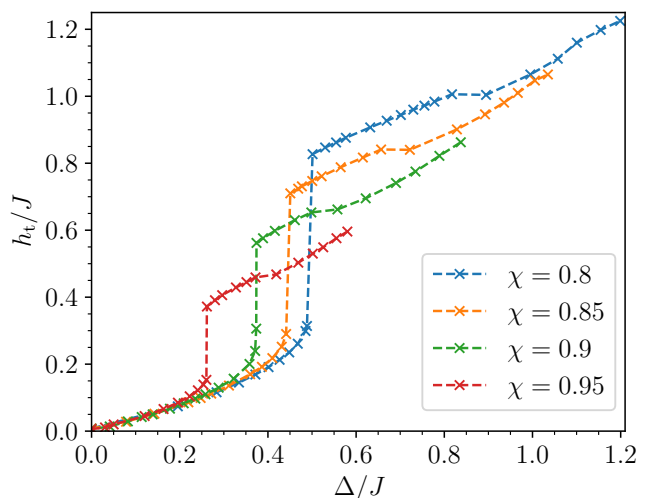


FIG. 16. Threshold magnetic field h_t vs. temperature for various anisotropies. The data is obtained for a system size $L = 200$. The jump occurs for $\chi = 0.95$ at $T = 0.6215J$ with $T_N = 0.652J$, for $\chi = 0.9$ at $T = 0.6775J$ with $T_N = 0.704J$, for $\chi = 0.85$ at $T = 0.7065J$ with $T_N = 0.725J$, and for $\chi = 0.8$ at $T = 0.7225J$ with $T_N = 0.732J$.

at low temperatures where the sublattice magnetization is considerably more robust.

In view of the discontinuity the imminent next question concerns the origin of this jump. To this end, we show in Fig. 17 the full temporal evolution of $m(t)$ for two temperatures: one is just below the jump, i.e., with an effective spin gap Δ slightly larger than the value at the jump and the other temperature just above the jump, i.e., with an effective spin gap slightly smaller than the jump value. Both panels show successful switching for some magnetic fields. But for the lower temperature (larger Δ) the magnetization only switches for large fields at times $t \approx 6J^{-1}$. For the larger temperature (smaller Δ) the magnetization also switches for low fields at times $t \approx 17J^{-1}$. At these times, the lower temperature does not yet allow for a sign change of the magnetization. Thus, the jump of the instant in time at which switching can be detected explains in turn the jump in the threshold fields.

V. CONCLUSIONS

Controlling the magnetization of long-range ordered quantum magnets is a key element in data storage in nanoscale domains. The magnetization orientation in such a domain serves as a bit. So far, it is realized and employed for ferromagnets. But it is established that quantum antiferromagnets display important advantages. They do not have stray fields which oppose close packing of the domains of magnetization, i.e., the bits. In addition, the generic time scales are shorter by three orders of magnitude in comparison to generic ferromag-

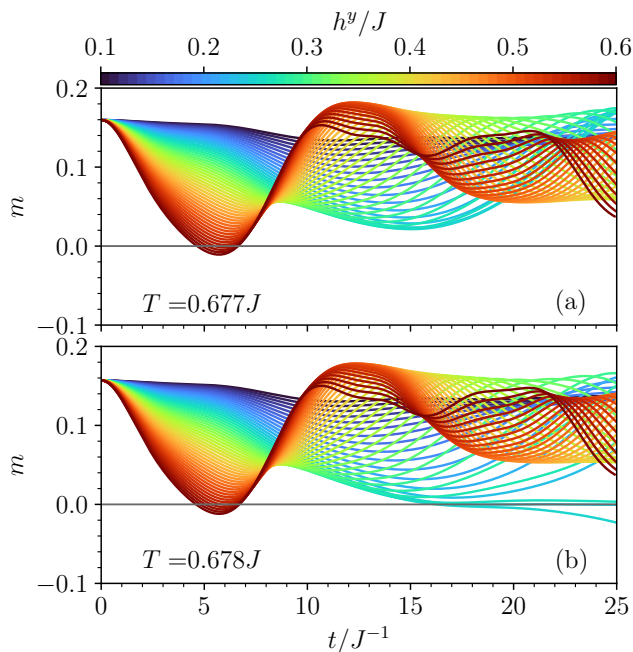


FIG. 17. Both panels show the full temporal evolution $m(t)$ for $\chi = 0.9$ for two very close values of the temperature of which one is just below (panel (a)) the temperature where the jump of h_t occurs and the other just above (panel (b)). There is a sign change in $m(t)$ in panel (a) at around $t \approx 6J^{-1}$ for larger fields. But note the additional change of sign in $m(t)$ in panel (b) at a larger time $t \approx 17J^{-1}$ for lower fields. This is responsible for a sudden change of the threshold field.

nets.

For these reasons, we investigated the switching of the antiferromagnetic sublattice magnetization in an anisotropic easy-axis Heisenberg antiferromagnet. We aimed at the development of a suitable microscopic quantum approach to describe this phenomenon. For simplicity, we studied the model on a square lattice. The aim was to go beyond the description of the magnetizations on the two sublattices by two classical vectors (vector model). We intended to base our approach on the quantum model which captures all leading quantum and thermal effects. Such a model has to comprise all the magnetic modes, i.e., a spin-wave description was required. Addressing all modes allows one to deal with dephasing of the modes in the course of switching as well as with finite temperature effects. These important effects are missed otherwise.

But the showstopper of conventional spin-wave theories is that they only capture the fluctuations around one of the degenerate ground states. Yet for the purpose of switching from one ground state (up-down on sublattice A-B) to the other (down-up), this is obviously not sufficient. Hence we resorted to the Schwinger boson description which captures all degenerate ordered states as well as the disordered ones. We use the established mean-field description which reproduces the result of the usual self-

consistent spin-wave theories in equilibrium based on the Holstein-Primakoff or the Dyson-Maleev representations.

We computed the spin gap within the Schwinger mean-field theory [18] and found results which agree with the reliable results from other techniques if the mean-field gap is scaled down by a factor ≈ 1.3 . This is a very satisfying result in view of the simplicity of the mean-field approach and the low dimensionality of the system. Similarly, the mean-field temperature T_N in the Ising limit agrees with the rigorous result from Onsager [32] within 30%.

Using the equilibrium expectation values as starting values we computed solutions of the Heisenberg equations of motions for the expectation values. In particular, we calculated the temporal evolution $m(t)$ upon application of a uniform transverse magnetic field which induces a Larmor precession. The magnetization in the isotropic model is rotated without loss of coherence and for arbitrarily weak fields. In the anisotropic case, however, an activation energy needs to be overcome. For weak magnetic fields h , no switching is possible; only weak oscillations below the equilibrium magnetization are induced. Above a threshold value h_t switching is possible, but the coherence of all the involved magnetic modes is deteriorating. Thus, for fields just above the threshold only a single switching is possible while for large control fields several swaps $m_0 \leftrightarrow -m_0$ can be realized. The threshold fields h_t at zero temperature agree almost quantitatively with the spin gap. The larger the spin gap the more robust the magnetic order is.

Analyzing the time t_π needed to perform (or to fail) a swap displays a logarithmic divergence at the threshold value, both from above and from below. This behavior coincides precisely with the time needed for a massive particle to overcome an energy barrier. This means that the antiferromagnetic magnetization disposes of an inertia in its dynamics as was observed both experimentally and theoretically in a classical vector model before [13].

Upon increasing the temperature the equilibrium magnetization and the effective spin gap decreases towards the Néel temperature where both vanish. Thus, it is not surprising that the threshold magnetic field required for switching decreases upon increasing temperature and vanishes also at T_N . Our model including the leading quantum and thermal effects confirms this expectation quantitatively. The relation between temperature or equivalently the effective spin gap and the threshold field is monotonic. Unexpectedly, however, we found a discontinuity in the threshold fields. At an intermediate value of the effective spin gap Δ the required minimum field suddenly decreases by a finite amount. Due to the square root laws $\Delta \propto \sqrt{T_N - T}$ this spin gap value corresponds to temperatures which are close to the transition temperature T_N . We could trace the origin of the jump to the full temporal evolution of the magnetization $m(t)$ during the switching. The instant of time where $m(t)$ changes sign jumps as well to longer times for lower fields.

What is the implication for experiment? As pointed out above, many parameters need to be taken into account. If we assume $J = 10$ meV and a small anisotropy $\chi \approx 0.99$ and/or a temperature rather close to the Néel temperature, the threshold field corresponds roughly to $0.05J = 0.5$ meV which corresponds for $g = 2$ to about 5 Tesla. Note that the spin gaps and thus threshold fields are likely to be 30% lower than the mean-field approach predicts. This is still a large field, but it is certainly realizable in a laboratory. Hence, we think that our results provide an interesting and quantitative guideline for future experiments. According to our findings the temperature dependence of the switching merits close inspection in particular.

The theoretical outlook comprises a large scope of promising extensions. Clearly, the present calculation can be extended to three dimensions and also to many other lattices. Certainly, other bipartite lattices can be treated in the very same fashion, but also frustrated lattices displaying long-range order such as the triangular

lattice [33] can be tackled. One can also apply the approach to models with anisotropies beyond easy-axis, for instance with a four-fold rotation symmetry of the magnetizations. Furthermore, time-dependent control fields can be considered as well so that a plethora of fundamentally interesting as well as practically relevant issues such as the influence of nanostructured confinement, are open for further investigation using the approach advocated here.

ACKNOWLEDGMENTS

We thank Davide Bossini for drawing our attention to this topic and Christoph Lange for very useful discussions. We gratefully acknowledge financial support by the German Research Foundation (DFG) in project UH 90-14/1 (GSU) and in TRR 160 (AK). Furthermore, KB thanks the Studienstiftung des Deutschen Volkes for funding.

-
- [1] L. F. Néel, Magnetism and the Local Molecular Field – Nobel Lecture (1970).
- [2] P. K. Misra, *Physics of Condensed Matter*, 1st ed. (Academic Press, Boston, 2011).
- [3] O. Gomonay, T. Jungwirth, and J. Sinova, Concepts of antiferromagnetic spintronics, *Physica Status Solidi - Rapid Research Letters* **11**, 1700022 (2017).
- [4] C. P. Chen and C. Zhang, Data-intensive applications, challenges, techniques and technologies: A survey on big data, *Information Sciences* **275**, 314 (2014).
- [5] M. Hilbert and P. López, The world’s technological capacity to store, communicate, and compute information, *Science* **332**, 60 (2011).
- [6] S. Loth, S. Baumann, C. P. Lutz, D. M. Eigler, and A. J. Heinrich, Bistability in atomic-scale antiferromagnets, *Science* **335**, 196 (2012).
- [7] E. V. Gomonay and V. M. Loktev, Spintronics of antiferromagnetic systems (review article), *Low Temperature Physics* **40**, 17 (2014).
- [8] T. Kampfrath, A. Sell, G. Klatt, A. Pashkin, S. Mährlein, T. Dekorsy, M. Wolf, M. Fiebig, A. Leitenstorfer, and R. Huber, Coherent terahertz control of antiferromagnetic spin waves, *Nature Photonics* **5**, 31 (2011).
- [9] T. Jungwirth, X. Marti, P. Wadley, and J. Wunderlich, Antiferromagnetic spintronics, *Nature Nanotechnology* **11**, 231 (2016).
- [10] L. Baldrati, A. Ross, T. Niizeki, C. Schneider, R. Ramos, J. Cramer, O. Gomonay, M. Filianina, T. Savchenko, D. Heinze, A. Kleibert, E. Saitoh, J. Sinova, and M. Kläui, Full angular dependence of the spin Hall and ordinary magnetoresistance in epitaxial antiferromagnetic NiO(001)/Pt thin films, *Physical Review B* **98**, 024422 (2018).
- [11] S. Y. Bodnar, Y. Skourski, O. Gomonay, J. Sinova, M. Kläui, and M. Jourdan, Magnetoresistance Effects in the Metallic Antiferromagnet Mn₂Au, *Physical Review Applied* **14**, 014004 (2020).
- [12] V. Grigorev, M. Filianina, S. Y. Bodnar, S. Sobolev, N. Bhattacharjee, S. Bommanaboyena, Y. Lytvynenko, Y. Skourski, D. Fuchs, M. Kläui, M. Jourdan, and J. Demsar, Optical Readout of the Néel Vector in the Metallic Antiferromagnet Mn₂Au, *Physical Review Applied* **16**, 014037 (2021).
- [13] A. V. Kimel, B. A. Ivanov, R. V. Pisarev, P. A. Usachev, A. Kirilyuk, and T. Rasing, Inertia-driven spin switching in antiferromagnets, *Nature Physics* **5**, 727 (2009).
- [14] R. Cheng, M. W. Daniels, J.-G. Zhu, and D. Xiao, Ultrafast switching of antiferromagnets via spin-transfer torque, *Physical Review B* **91**, 064423 (2015).
- [15] H. V. Gomonay and V. M. Loktev, Spin transfer and current-induced switching in antiferromagnets, *Physical Review B* **81**, 144427 (2010).
- [16] J. Železný, H. Gao, K. Výborný, J. Zemen, J. Mašek, A. Manchon, J. Wunderlich, J. Sinova, and T. Jungwirth, Relativistic Néel-Order Fields Induced by Electrical Current in Antiferromagnets, *Physical Review Letters* **113**, 157201 (2014).
- [17] P. Wadley, B. Howells, J. Železný, C. Andrews, V. Hills, R. P. Campion, V. Novák, K. Olejník, F. Maccheronzi, S. S. Dhesi, S. Y. Martin, T. Wagner, J. Wunderlich, F. Freimuth, Y. Mokrousov, J. Kuneš, J. S. Chauhan, M. J. Grzybowski, A. W. Rushforth, K. W. Edmonds, B. L. Gallagher, and T. Jungwirth, Electrical switching of an antiferromagnet, *Science* **351**, 587 (2016).
- [18] A. Auerbach, *Interacting Electrons and Quantum Magnetism*, Graduate Texts in Contemporary Physics (Springer, New York, 1994).
- [19] T. Holstein and H. Primakoff, Field dependence of the intrinsic domain magnetization of a ferromagnet, *Physical Review* **58**, 1098 (1940).
- [20] F. J. Dyson, General theory of spin-wave interactions, *Physical Review* **102**, 1217 (1956).
- [21] S. V. Maleev, Scattering of slow neutrons in ferromagnets, *Soviet Physics JETP* **6**, 766 (1958).

- [22] J. Schwinger, On angular momentum, US Atomic Energy Commission 10.2172/4389568 (1952).
- [23] D. P. Arovas and A. Auerbach, Functional integral theories of low-dimensional quantum Heisenberg models, *Physical Review B* **38**, 316 (1988).
- [24] A. Auerbach and D. P. Arovas, Spin dynamics in the square-lattice antiferromagnet, *Physical Review Letters* **61**, 617 (1988).
- [25] L. O. Manuel and H. A. Ceccatto, Magnetic and quantum disordered phases in triangular-lattice Heisenberg antiferromagnets, *Physical Review B* **60**, 9489 (1999).
- [26] T. N. De Silva, M. Ma, and F. C. Zhang, Pathology of Schwinger boson mean-field theory for Heisenberg spin models, *Physical Review B* **66**, 104417 (2002).
- [27] M. Raykin and A. Auerbach, $1/N$ expansion and spin correlations in constrained wave functions, *Physical Review B* **47**, 5118 (1993).
- [28] M. Mathur, I. Raychowdhury, and R. Anishetty, SU(N) irreducible Schwinger bosons, *Journal of Mathematical Physics* **51**, 093504 (2010).
- [29] N. D. Mermin and H. Wagner, Absence of Ferromagnetism or Antiferromagnetism in One- or Two-Dimensional Isotropic Heisenberg Models, *Physical Review Letters* **17**, 1133 (1966).
- [30] E. A. Ghioldi, A. Mezio, L. O. Manuel, R. R. P. Singh, J. Oitmaa, and A. E. Trumper, Magnons and excitation continuum in XXZ triangular antiferromagnetic model: Application to $\text{Ba}_3\text{CoSb}_2\text{O}_9$, *Physical Review B* **91**, 134423 (2015).
- [31] M. R. Walther, D.-B. Hering, G. S. Uhrig, and K. P. Schmidt, Continuous similarity transformation for critical phenomena: easy-axis antiferromagnetic XXZ model, *Physical Review Research* **5**, 013132 (2023).
- [32] L. Onsager, Crystal Statistics. I. A Two-Dimensional Model with an Order-Disorder Transition, *Physical Review* **65**, 117 (1944).
- [33] A. L. Chernyshev and M. E. Zhitomirsky, Spin waves in a triangular lattice antiferromagnet: Decays, spectrum renormalization, and singularities, *Physical Review B* **79**, 144416 (2009).

Appendix A: Sublattice magnetization for the isotropic case

In this appendix, we show how spontaneous symmetry breaking manifests itself in the Schwinger boson representation as Bose-Einstein condensation [18] and how the condensate is related to a finite sublattice magnetization, see Eq. (22a) in the main text. We consider the isotropic antiferromagnetic two-dimensional square lattice at zero temperature in the thermodynamic limit.

In order to capture the spontaneous symmetry breaking we initially add an alternating magnetic field h_{alt}^z in z -direction to the system by means of an alternating Zeeman term (5). Once the thermodynamic limit is taken, this external field will be decreased to zero. The Hamiltonian reads

$$\mathcal{H} = \mathcal{H}_0 = \mathcal{H}_0 - \frac{h_{\text{alt}}^z}{2} \sum_i \left(a_i^\dagger a_i - b_i^\dagger b_i \right), \quad (\text{A1})$$

where \mathcal{H}_0 denotes the unperturbed mean-field Hamiltonian (15). The alternation is no longer manifest because we effectively rotated the spins on every second site around S^y . Since a - and b -bosons are no longer equivalent in (A1) the two dispersions differ

$$\mathcal{H} = E_{\text{MF}} - N\lambda + \sum_{\mathbf{k}} \left\{ \omega_{\mathbf{k}}^\alpha \left(\alpha_{\mathbf{k}}^\dagger \alpha_{\mathbf{k}} + \frac{1}{2} \right) + \omega_{\mathbf{k}}^\beta \left(\beta_{\mathbf{k}}^\dagger \beta_{\mathbf{k}} + \frac{1}{2} \right) \right\} \quad (\text{A2})$$

with

$$\omega_{\mathbf{k}}^\alpha = \sqrt{(\lambda - h_{\text{alt}}^z/2)^2 - (2A\gamma_{\mathbf{k}})^2}, \quad (\text{A3a})$$

$$\omega_{\mathbf{k}}^\beta = \sqrt{(\lambda + h_{\text{alt}}^z/2)^2 - (2A\gamma_{\mathbf{k}})^2}. \quad (\text{A3b})$$

Note that for a positive external field, the dispersion of the α -boson is lower and hence the condensation of α -bosons is to be expected.

The spontaneous sublattice magnetization results from

$$m_0 = \lim_{h_{\text{alt}}^z \rightarrow 0^+} m(h_{\text{alt}}^z) \quad \text{with} \quad (\text{A4a})$$

$$m(h_{\text{alt}}^z) = \lim_{N \rightarrow \infty} \frac{1}{2N} \sum_i \left(\langle a_i^\dagger a_i \rangle - \langle b_i^\dagger b_i \rangle \right). \quad (\text{A4b})$$

Explicit calculation of the average boson number and of the sublattice magnetization yields

$$S + \frac{1}{2} = \frac{1}{4N} \sum_{\mathbf{k}} \left(\frac{\lambda - h_{\text{alt}}^z/2}{\omega_{\mathbf{k}}^\alpha} + \frac{\lambda + h_{\text{alt}}^z/2}{\omega_{\mathbf{k}}^\beta} \right), \quad (\text{A5a})$$

$$m(h_{\text{alt}}^z) = \frac{1}{4N} \sum_{\mathbf{k}} \left(\frac{\lambda - h_{\text{alt}}^z/2}{\omega_{\mathbf{k}}^\alpha} - \frac{\lambda + h_{\text{alt}}^z/2}{\omega_{\mathbf{k}}^\beta} \right). \quad (\text{A5b})$$

Since we expect the condensation of the α -bosons, we substitute $(\lambda - h_{\text{alt}}^z/2)^2 = 4A^2(1 + \kappa^2)$ with $\kappa = \tilde{f}/N$ analogous to what we did in the main text. This implies

$$\omega_{\mathbf{k}}^\alpha = 2A\sqrt{1 + \kappa^2 - \gamma_{\mathbf{k}}^2}, \quad (\text{A6a})$$

$$\omega_{\mathbf{k}}^\beta = 2A\sqrt{1 + \kappa^2 + \frac{\lambda h}{2A^2} - \gamma_{\mathbf{k}}^2}. \quad (\text{A6b})$$

The dispersion $\omega_{\mathbf{k}}^\alpha$ becomes gapless in the thermodynamic limit which is necessary for the condensation of the α -bosons. Transforming the sums in (A5a) and (A5b) into integrals plus a contribution at $\mathbf{k} = (0, 0)$ and (π, π) reveals that *no* such extra contribution occurs for the β -bosons (second fractions in the brackets in Eqs. (A5)) because at any finite h_{alt}^z , their dispersion does not vanish. Thus, their sum converges smoothly to the integral contribution. For the α -bosons, however, we obtain the additional contribution $2/(4\tilde{f}) = 1/(2\tilde{f})$ accounting for the prefactors of the sums in (A5). The integrals for the α - and the β -bosons become the same for $h_{\text{alt}}^z \rightarrow 0$ and thus cancel. Eventually, we obtain

$$m_0 = 1/(2\tilde{f}). \quad (\text{A7})$$

This relates the spontaneously occurring sublattice magnetization directly to the condensate fraction, here of the α -bosons.

In order to arrive at Eq. (22a) we recall that there the choice $\kappa = f/N$ referred to the *disordered* case where *both* bosons, α and β , condense yielding a condensate contribution $\propto 1/f$. Thus, if only *one* kind of boson condenses, it must contribute double the amount, hence $\tilde{f} = f/2$ due to the inverse proportionality. Hence $m_0 = 1/f$ ensues.

For an explicit calculation, one can subtract the two equations (A5a) and (A5b)

$$S + \frac{1}{2} - m_0 = \frac{1}{8\pi^2} \int_{\text{BZ}} dk^2 \frac{1}{\sqrt{1 - \gamma_{\mathbf{k}}^2}}. \quad (\text{A8})$$

This eliminates the macroscopic contributions from $\mathbf{k} = (0, 0)$ and (π, π) . Then we set $h_{\text{alt}}^z = 0$ to reach the above equation. Solving for m_0 yields

$$m_0 = S + \frac{1}{2} - \frac{1}{8\pi^2} \int_{\text{BZ}} dk^2 \frac{1}{\sqrt{1 - \gamma_{\mathbf{k}}^2}} \quad (\text{A9a})$$

$$= S - 0.1966, \quad (\text{A9b})$$

where we evaluated the integral numerically for the last line. Comparing the first line (A9a) with half the equation (21b) one arrives at $m_0 = 1/f$ as stated in Eq. (22a). This underlines the above argument that $\tilde{f} = f/2$ holds in the comparison of the long-range ordered ground state with the disordered ground state. In summary, Eq. (22b) is derived.

Appendix B: Approximating the thermodynamic limit for the isotropic case

A finite system is used to approximate an infinitely large lattice in order to obtain a numerically feasible set of differential equations. However, unlike the infinite or anisotropic case, finite two-dimensional isotropic spin lattices, i.e., for $\chi = 1$, do not display magnetic order. Therefore, an infinitesimal magnetic field h_{alt}^z in z -direction is added, which enforces an initial magnetic order to make the finite isotropic system have the same magnetization as obtained in (A9b), which is $m_{0,\text{iso}} = 0.3034$ for $S = \frac{1}{2}$.

In order to determine a suitable value of the magnetic field, the initial magnetization $m(h_{\text{alt}}^z)$ of the isotropic system for various system sizes and spin $S = \frac{1}{2}$ is plotted against the scaled field h_{alt}^z in Fig. 18. All curves demonstrate that a small field scaling $\propto \frac{1}{N}$ is already sufficient to generate the magnetic order. The larger the system, the more the magnetization curve converges to the discontinuous curve of an infinitely large system, where the magnetization persists even for $h_{\text{alt}}^z \rightarrow 0^+$. The inset shows that the sublattice magnetization $m(h_{\text{alt}}^z)$ corresponds to the desired value $m_{0,\text{iso}} = 0.3034$ for $h_{\text{alt}}^z = 1.329 JN^{-1}$. We find it remarkable and reassuring

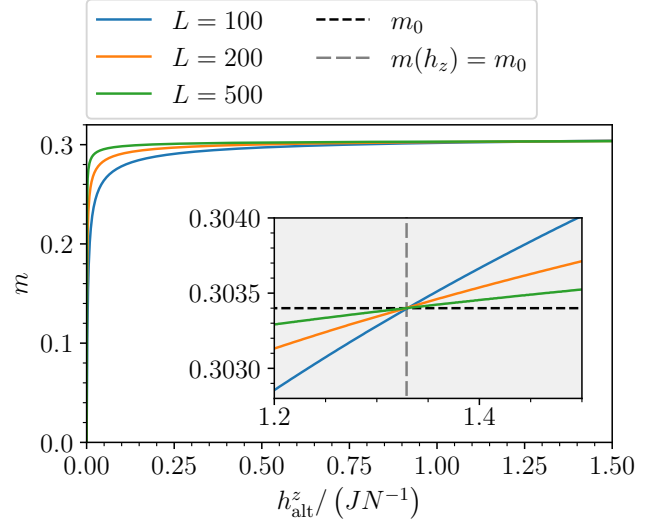


FIG. 18. The initial magnetization m of the isotropic system, i.e., $\chi = 1$, as a function of a small field h_{alt}^z for different system sizes. Magnetic order is already obtained for small fields, recall $N = L^2$. The desired initial magnetization $m_{0,\text{iso}} = 0.3034$ is reached for $h_{\text{alt}}^z = 1.329 JN^{-1}$, as shown in the inset. Around this value, the curves for the various system sizes intersect.

that in the close vicinity of this value, the curves for various L almost intersect. They do not intersect precisely in one point, but in a very narrow region. Still, this corroborates our way to approximate the thermodynamic limit by finite clusters.

Appendix C: Zero temperature equations for the anisotropic case

For the condensation of the α -bosons, the dispersion ω^- should become gapless for an infinitely large system at zero temperature, which is why

$$\lambda^2 = C_-^2 (1 + \kappa^2) \quad (\text{C1})$$

is chosen with $\kappa = \frac{\tilde{f}}{N}$. We use \tilde{f} because only one of the two boson flavors is to condense. As before, this yields the dispersions

$$\omega_{\mathbf{k}}^- = C_- \sqrt{1 + \kappa^2 - \gamma_{\mathbf{k}}^2}, \quad (\text{C2a})$$

$$\omega_{\mathbf{k}}^+ = \sqrt{C_-^2 (1 + \kappa^2) - C_+^2 \gamma_{\mathbf{k}}^2}. \quad (\text{C2b})$$

It is important to note that only $\omega_{\mathbf{k}}^+$ describes the true spin-wave spectrum for $T = 0$ because the operator of the condensed boson can be replaced $\alpha_{\mathbf{k}}^{(\dagger)} \rightarrow \sqrt{Nm_0}/2$. In the thermodynamic limit $N \rightarrow \infty$, the sums in (33) become integrals as before plus the contributions from

$\mathbf{k} = (0, 0)$ and (π, π)

$$2S = \frac{1}{8\pi^2} \int_{\text{BZ}} dk^2 \left[\frac{1}{\sqrt{1-\gamma_{\mathbf{k}}^2}} + \frac{C_-}{\sqrt{C_-^2 - C_+^2 \gamma_{\mathbf{k}}^2}} \right] + \frac{1}{\tilde{f}} - 1, \quad (\text{C3a})$$

$$A = \frac{1}{8\pi^2} \int_{\text{BZ}} dk^2 \gamma_{\mathbf{k}}^2 \left[\frac{1}{\sqrt{1-\gamma_{\mathbf{k}}^2}} + \frac{C_+}{\sqrt{C_-^2 - C_+^2 \gamma_{\mathbf{k}}^2}} \right] + \frac{1}{\tilde{f}}, \quad (\text{C3b})$$

$$B = \frac{1}{8\pi^2} \int_{\text{BZ}} dk^2 \gamma_{\mathbf{k}}^2 \left[\frac{1}{\sqrt{1-\gamma_{\mathbf{k}}^2}} - \frac{C_+}{\sqrt{C_-^2 - C_+^2 \gamma_{\mathbf{k}}^2}} \right] + \frac{1}{\tilde{f}}. \quad (\text{C3c})$$

Finally, (C3b) and (C3c) are each subtracted from (C3a), yielding the two equations

$$2S + 1 - A = \frac{1}{8\pi^2} \int_{\text{BZ}} dk^2 \left[\frac{1-\gamma_{\mathbf{k}}^2}{\sqrt{1-\gamma_{\mathbf{k}}^2}} + \frac{C_- - C_+ \gamma_{\mathbf{k}}^2}{\sqrt{C_-^2 - C_+^2 \gamma_{\mathbf{k}}^2}} \right], \quad (\text{C4a})$$

$$2S + 1 - B = \frac{1}{8\pi^2} \int_{\text{BZ}} dk^2 \left[\frac{1-\gamma_{\mathbf{k}}^2}{\sqrt{1-\gamma_{\mathbf{k}}^2}} + \frac{C_- + C_+ \gamma_{\mathbf{k}}^2}{\sqrt{C_-^2 - C_+^2 \gamma_{\mathbf{k}}^2}} \right]. \quad (\text{C4b})$$

These equations allow us to determine A and B . The results are shown in Fig. 19. The Lagrange multiplier λ is implicitly fixed by the condition that the α -bosons condense and their dispersion is massless.

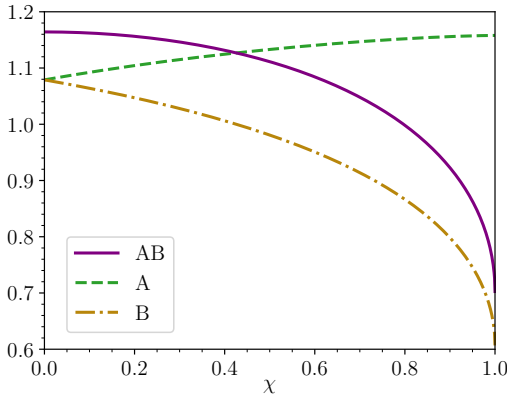


FIG. 19. Expectation values A and B and their product in equilibrium plotted as a function of the anisotropy χ . These values enter in the determination of the spin gap in Fig. 3 and of the magnetization in Fig. 4.

To determine the sublattice magnetization from Eq. (34) we consider its thermodynamic limit $N \rightarrow \infty$

$$m_0 = \frac{1}{16\pi^2} \int_{\text{BZ}} dk^2 \left[\frac{1}{\sqrt{1-\gamma_{\mathbf{k}}^2}} - \frac{C_-}{\sqrt{C_-^2 - C_+^2 \gamma_{\mathbf{k}}^2}} \right] + \frac{1}{2\tilde{f}}. \quad (\text{C5})$$

Subtracting this equation from half the Eq. (C3a) yields

$$S + \frac{1}{2} - m_0 = \frac{1}{8\pi^2} \int_{\text{BZ}} dk^2 \frac{C_-}{\sqrt{C_-^2 - C_+^2 \gamma_{\mathbf{k}}^2}} \quad (\text{C6})$$

eliminating the condensate contribution $\propto 1/\tilde{f}$. Solving the last equation for m_0 yields Eq. (35).

Appendix D: Overcoming a potential barrier

Here we motivate by a classical example why a logarithmic singularity is to be expected in Fig. 11 and why this is an indication of inertia. For this purpose a potential $V(x) = -\frac{1}{2}\gamma^2 x^2$ is considered as shown in Fig. 20. We want to know how long it takes a mass to move over this potential barrier. For the sake of simplicity, the mass is set to $m = 1$. The Hamilton function of the system reads

$$\mathcal{H} = \frac{p^2}{2} - \frac{1}{2}\gamma^2 x^2. \quad (\text{D1})$$

We highlight that the existence of the kinetic energy reflects the existence of inertia. The resulting equation of motion reads

$$\ddot{x} - \gamma^2 x = 0, \quad (\text{D2})$$

and has the general solution

$$x(t) = F \cosh(\gamma t) + G \sinh(\gamma t). \quad (\text{D3})$$

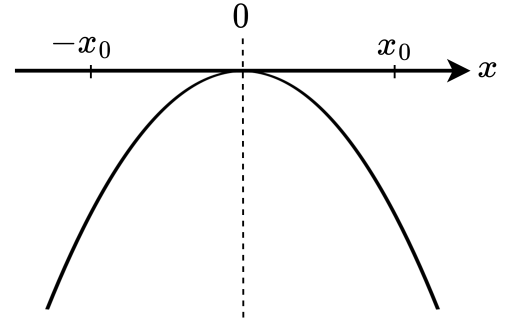


FIG. 20. The considered potential barrier $V(x) = -\frac{1}{2}\gamma^2 x^2$. The points $\pm x_0$ are used to indicate whether the barrier has been overcome or not.

The initial conditions are $x(0) = x_0 > 0$ and $\dot{x}(0) = -v_0 < 0$. Thus, we find $F = x_0$ and $G = -v_0/\gamma$. The total energy of the system takes the value

$$2E = v_0^2 - \gamma^2 x_0^2 = (\gamma G)^2 - (\gamma F)^2. \quad (\text{D4})$$

The marginal case is given for $E = 0$ because in this case the kinetic energy disappears exactly when the potential maximum is reached. This corresponds to $F = -G$ implying

$$x(t) = x_0 (\cosh(\tau) - \sinh(\tau)) = x_0 e^{-\tau} \quad (\text{D5})$$

with $\tau := \gamma t$. Note that the solution $F = G$ is discarded because of the restrictions $F > 0$ and $G < 0$. The maximum at $x = 0$ is thus reached exponentially slowly. Next, we consider a small deviation $G = -x_0(1 + 2\delta)$ from the marginal case. For $\delta > 0$, the total energy is positive, and therefore the potential barrier can be passed. We calculate the necessary time when the point $-x_0$ is reached

$$-x_0 = x_0 e^{-t} - \delta x_0 (e^\tau - e^{-\tau}) \quad (\text{D6a})$$

$$\Leftrightarrow 0 = \delta(y^2 - 1) - y - 1 \quad \text{with } y := e^\tau \quad (\text{D6b})$$

$$\Leftrightarrow y = \frac{1}{2\delta} + \sqrt{\frac{1}{4\delta^2} + \frac{1+\delta}{\delta}} \quad (\text{D6c})$$

$$= 1 + \frac{1}{\delta} + \mathcal{O}(\delta^2). \quad (\text{D6d})$$

The other solution of the quadratic equation is negative and therefore not a physical solution. The position $-x_0$ is reached at the time

$$\gamma t = \tau = -\ln|\delta| + \delta + \mathcal{O}(\delta^2). \quad (\text{D7})$$

For $\delta < 0$, the total energy is negative, and therefore the potential barrier cannot be passed; the passage fails. In this case, we calculate the time it takes to get back to

the point x_0

$$x_0 = x_0 e^{-\tau} + |\delta|x_0 (e^\tau - e^{-\tau}) \quad (\text{D8a})$$

$$\Leftrightarrow 0 = y - 1 - |\delta| (y^2 - 1) \quad (\text{D8b})$$

$$\Leftrightarrow y = \frac{1}{2|\delta|} + \sqrt{\frac{1}{4|\delta|^2} - \frac{1-|\delta|}{\delta}} \quad (\text{D8c})$$

$$= \frac{1}{|\delta|} - 1 + \mathcal{O}(\delta^2). \quad (\text{D8d})$$

Again, the other solution of the quadratic equation is not physically significant. So the time for reaching x_0 again is

$$\gamma t = \tau = -\ln|\delta| + \delta + \mathcal{O}(\delta^2). \quad (\text{D9})$$

Remarkably, the same result ensues for succeeding to pass the barrier as for failing to pass it. In both cases, a logarithmic divergence of the time occurs just as we observed for switching the sublattice magnetization in Figs. 10 and 11. Note that the fitted prefactors in Eqs. (45) and (46) are very close to each other as one expects from the classical calculation presented above. Note that this symmetry is perfectly reflected by the curves in Fig. 10 for magnetic fields just above and just below the threshold value which are mirror images of one another in the vicinity of the first extremum for $t > 0$.

In addition, we observe in the solution (D5) as well as in the curves in Fig. 10 for the cases in the vicinity of the threshold that most of the time is spent around the energy maximum $x \approx 0$ or $m \approx 0$, respectively. This underlines that we are dealing with a process governed by inertia: What matters is the maximum *energy* that the switching term can provide. In contrast, a process without inertia, governed by friction, would spend most of the time close to the point where the maximum *force* is required. This is certainly not the case for $m \approx 0$, but rather would be around $m \approx \pm m_0/2$. Thus, the curves in Fig. 10 underline the conclusion that the magnetization dynamics in quantum antiferromagnets is governed by inertia.